JGP Journal of General Physiology

ARTICLE

L-type channel inactivation balances the increased peak calcium current due to absence of Rad in cardiomyocytes

Brooke M. Ahern[1], Andrea Sebastian[1], Bryana M. Levitan[1,2], Jensen Goh[1], Douglas A. Andres[3], and Jonathan Satin[1]

The L-type Ca^{2+} channel (LTCC) provides trigger calcium to initiate cardiac contraction in a graded fashion that is regulated by L-type calcium current ($I_{Ca,L}$) amplitude and kinetics. Inactivation of LTCC is controlled to fine-tune calcium flux and is governed by voltage-dependent inactivation (VDI) and calcium-dependent inactivation (CDI). Rad is a monomeric G protein that regulates $I_{Ca,L}$ and has recently been shown to be critical to β-adrenergic receptor (β-AR) modulation of $I_{Ca,L}$. Our previous work showed that cardiomyocyte-specific Rad knockout (cRadKO) resulted in elevated systolic function, underpinned by an increase in peak $I_{Ca,L}$, but without pathological remodeling. Here, we sought to test whether Rad-depleted LTCC contributes to the fight-or-flight response independently of β-AR function, resulting in $I_{Ca,L}$ kinetic modifications to homeostatically balance cardiomyocyte function. We recorded whole-cell $I_{Ca,L}$ from ventricular cardiomyocytes from inducible cRadKO and control (CTRL) mice. The kinetics of $I_{Ca,L}$ stimulated with isoproterenol in CTRL cardiomyocytes were indistinguishable from those of unstimulated cRadKO cardiomyocytes. CDI and VDI are both enhanced in cRadKO cardiomyocytes without differences in action potential duration or QT interval. To confirm that Rad loss modulates LTCC independently of β-AR stimulation, we crossed a β_1,β_2-AR double-knockout mouse with cRadKO, resulting in a Rad-inducible triple-knockout mouse. Deletion of Rad in cardiomyocytes that do not express β_1,β_2-AR still yielded modulated $I_{Ca,L}$ and elevated basal heart function. Thus, in the absence of Rad, increased Ca^{2+} influx is homeostatically balanced by accelerated CDI and VDI. Our results indicate that the absence of Rad can modulate the LTCC without contribution of β_1,β_2-AR signaling and that Rad deletion supersedes β-AR signaling to the LTCC to enhance in vivo heart function.

Introduction

The L-type calcium channel (LTCC) is a heteromultimeric protein complex that governs the entry of calcium necessary to initiate a contraction, and the LTCC contributes to the cardiac action potential (AP) plateau phase (Breijo-Marquez, 2012). Cardiomyocyte LTCC activity is tightly regulated to prevent calcium overload (Bers, 2002) and afterdepolarizations of the AP (January et al., 1988; January and Riddle, 1989). The decay kinetics of $I_{Ca,L}$ is a key point of control. Inactivation of the LTCC occurs by two distinct mechanisms: calcium-dependent inactivation (CDI) and voltage-dependent inactivation (VDI; Breijo-Marquez, 2012; Pelzer et al., 1990). The early peak of L-type calcium current ($I_{Ca,L}$) triggers CICR from the SR that is essential for excitation–contraction coupling; calcium released from the SR or entering through the channel itself binds to calmodulin (CaM) prebound to the EF hand of the C terminus of the main pore-forming subunit of the LTCC (Zühlke et al., 1999). Ca^{2+}-CaM complexed within the LTCC causes a conformational change to induce CDI (Peterson et al., 1999; Tadross et al., 2008; Alseikhan et al., 2002; Zamponi, 2003). In addition, $I_{Ca,L}$ decay occurs by VDI contemporaneously with the plateau phase of the AP (Findlay, 2002a; Findlay, 2002c; Findlay, 2002b; Findlay, 2004). Under basal conditions, the decay of $I_{Ca,L}$ demonstrates nonexponential decay with relatively early, fast components and late, slow components (Mahajan et al., 2008; Madhvani et al., 2011; Karagueuzian et al., 2017; Madhvani et al., 2015). It is generally accepted that CDI contributes to the early, fast component and that the late, slow component is dominated by VDI (Findlay, 2004; Morales et al., 2019). Other studies claim that VDI contributes to both components but is dampened when calcium influx increases (Findlay, 2002a; Findlay, 2004; Findlay, 2002c; Findlay, 2002b).

The regulation of LTCC decay becomes particularly critical when the channel is modulated upon β-adrenergic receptor

[1]Department of Physiology, University of Kentucky, Lexington, KY; [2]Gill Heart and Vascular Institute, University of Kentucky, Lexington, KY; [3]Department of Molecular and Cellular Biochemistry, University of Kentucky, Lexington, KY.

Correspondence to Jonathan Satin: jsatin1@uky.edu.

(β-AR) stimulation. During the fight-or-flight response, $I_{Ca,L}$ amplitude increases, voltage dependence of activation shifts to more negative potentials, and inactivation rates accelerate (Findlay, 2004; Morales et al., 2019; Bean et al., 1984; Morotti et al., 2012). Regulation of the LTCC by β-AR stimulation has been thoroughly investigated; yet, complete understanding remains elusive, especially in regard to how inactivation is accelerated. Many studies claim that CDI is the major contributor to $I_{Ca,L}$ decay under modulated conditions because elevated calcium influx leads to more calcium interaction with CaM (Findlay, 2004; Morales et al., 2019); however, increased $I_{Ca,L}$ due to overexpression of α_{1C}, the pore-forming subunit of the LTCC, or of voltage-gated calcium channel β_{2a} ($Ca_V\beta_{2a}$) did not alter decay kinetics compared with the controls (Muth et al., 1999; Chen et al., 2011). Others argue that inactivation is accelerated due to interactions of the N terminus and C terminus with each other or with other proteins (Lei et al., 2018; Benmocha Guggenheimer et al., 2016; Ivanina et al., 2000). Because β-AR stimulation initiates multiple molecular mechanisms, it is difficult to assess the main contributors to LTCC regulation (Pallien and Klussmann, 2020).

In recent studies, Rad has emerged as a major contributor to LTCC modulation (Ahern et al., 2019; Levitan et al., 2016; Liu et al., 2020). Rad is a member of the RGK subfamily of Ras-related small GTPases (Correll et al., 2008) and shares the common RGK protein property of profoundly inhibiting Ca_V1/Ca_V2 channel activity. Overexpression of Rad in heterologous expression systems potently inhibits $I_{Ca,L}$ in adult and embryonic ventricular myocytes (Finlin et al., 2003; Gunton et al., 2012; Magyar et al., 2012; Yang and Colecraft, 2013; Béguin et al., 2001). In vivo Rad deficiency promotes positive inotropy and is a critical determinant of current amplitude (Ahern et al., 2019) and modulation (Levitan et al., 2016; Liu et al., 2020). Our recent work showed that the absence of Rad from the channel complex results in increased LTCC activity that mirrors β-AR–modulated $I_{Ca,L}$ and accelerates $I_{Ca,L}$ decay (Ahern et al., 2019; Manning et al., 2013; Manning et al., 2015; Levitan et al., 2016). These findings were definitively supported using proximity biotinylation to show that under conditions of β-AR stimulation, PKA-mediated Rad phosphorylation alleviated constitutive inhibition caused by Rad association with the LTCC (Liu et al., 2020).

If Rad loss from the LTCC complex is essential for β-AR modulation of $I_{Ca,L}$, then the absence of Rad in the myocardium could serve as a novel tool to investigate LTCC regulation under modulated conditions without interfering contributions of other signaling pathways normally activated under β-AR stimulation. Using a cardiomyocyte-restricted Rad deletion mouse model, we revisited the hypothesis that modulation of the LTCC by β-AR stimulation is governed by the presence of Rad in the $Ca_V1.2$ macromolecular complex. Mechanistically, the absence of Rad yields increased inactivation to offset the increase in peak $I_{Ca,L}$. Here, we show that CDI and VDI are both accelerated in the absence of Rad. The combination of greater peak and accelerated kinetics conspires to prevent significant changes to AP duration (APD) or QT interval, despite large peak $I_{Ca,L}$. The preservation of Rad knockout instilled $I_{Ca,L}$ modulation in the absence of β-AR expression, thus showing that Rad imparts channel complex modulation independent of β-AR signaling. This work suggests that Rad–LTCC interactions may be a novel target for future therapeutics to confer systolic advantage.

Materials and methods

All experimental procedures and protocols were approved by the animal care and use committee of the University of Kentucky and conformed to the National Institutes of Health Guide for the Care and Use of Laboratory Animals.

Animal model

Mice lacking Rad expression ($RAD^{\Delta/\Delta}$; cardiomyocyte-specific Rad knockout [cRadKO]) were generated and characterized as previously described (Ahern et al., 2019). Transgenic animals were generated on a C57BL/6J background in the Transgenic Animal and Genome Editing Core at Cincinnati Children's Hospital Medical Center. Details are reported in Ahern et al. (2019). RAD deficiency was induced by a single intraperitoneal injection in control ($RAD^{fl/fl}$; CTRL) and experimental mice with tamoxifen dissolved in sunflower seed oil (40 mg/kg body weight). All mice received tamoxifen and were used >2 wk after tamoxifen treatment unless otherwise stated. This single tamoxifen injection protocol minimizes cardiomyopathological effects observed with multiday administration of tamoxifen. β_1-AR and β_2-AR double-knockout (dKO) mice were from The Jackson Laboratory (stock no. 003810; Rohrer et al., 1999). These mice were bred onto our $RAD^{fl/fl\text{-}MHC}$ animals to produce the $\beta_1\beta_2$-AR and Rad triple knockout (tKO) after administration of tamoxifen.

Ventricular myocyte isolation

Isolated ventricular cardiomyocytes were prepared as previously described (Magyar et al., 2012). Prior to heart excision, mice were anesthetized with ketamine + xylazine (90 + 10 mg/kg intraperitoneally). Hearts were excised from adult mice (3–7 mo of age) and immediately perfused on a Langendorff apparatus with a high-potassium Tyrode buffer and then digested with 5–7 mg Liberase (Roche). After digestion, atria were removed, and ventricular myocytes were mechanically dispersed. Calcium concentrations were gradually restored to physiological levels in a stepwise fashion, and only healthy quiescent ventricular myocytes were used for electrophysiological analysis within 12 h.

Electrophysiological recordings

$I_{Ca,L}$ was recorded in the whole-cell configuration of the patch-clamp technique as previously described (Magyar et al., 2012). All recordings were performed at room temperature (20–22°C). The pipette solution consisted of (in mmol/liter) 125 Cs-methanesulfonate, 15 TEA-Cl, 1 $MgCl_2$, 10 EGTA [or 10 1,2-bis(*o*-aminophenoxy)ethane-*N*,*N*,*N*′,*N*′-tetraacetic acid (BAPTA)], 5 HEPES, 5 Mg-ATP, and 5 phosphocreatine, pH 7.2. Physiological Tyrode bath solution contained (in mmol/liter) 140 NaCl, 5.4 KCl, 1.2 KH_2PO_4, 5 HEPES, 5.55 glucose, 1 $MgCl_2$, and 1.8 $CaCl_2$, pH 7.4. Once a cell was successfully patched, zero sodium bath solution was introduced into the chamber

containing (in mmol/liter): 150 NMDG, 2.5 $CaCl_2$, 1 $MgCl_2$, 10 glucose, 10 HEPES, and 5 4-aminopyridine, pH 7.2. Recordings of barium response were recorded in zero sodium bath solution containing 2.5 mmol/liter $BaCl_2$. Recordings of isoproterenol (ISO) response were recorded in zero sodium bath solution containing 300 nM ISO. Recordings of H89 were obtained from ventricular cardiomyocytes incubated in physiological Tyrode bath solution containing 2 µM H89 and then introduced to zero sodium bath solution also containing 2 µM H89. Traces were normalized to peak $I_{Ca,L}$, and then mean amplitude was measured at 30 ms and 150 ms after peak. Remaining current was then calculated by subtracting the mean amplitude from 1. AP recordings were performed in the physiological Tyrode bath solution as used for the other recordings. For AP recordings, the pipette solution contained (in mmol/liter) 115 K-glutamate, 45 KCl, 3 Mg-ATP, and 10 HEPES, pH 7.21 (KOH). All AP recordings were performed at room temperature (20–22°C).

Cytosolic Ca^{2+} transient recordings

Calcium transients were recorded from ventricular cardiomyocytes loaded with cell-permeable Fura-2 acetoxymethyl ester (Invitrogen) at 1.0 Hz to determine transient amplitude, upstroke velocity, and rate of decay. All measurements were made following >2 min of conditioning of 1-Hz field stimuli to induce a steady state. Transients were recorded at 1 Hz. To determine SR Ca^{2+} load, pacing was stopped, and cells received a focal puff of 10 mM caffeine. All Ca^{2+} transient data were analyzed using IonOptix IonWizard 6.3. Background fluorescence for F_{380} and F_{340} was determined from cell-free regions. Data are expressed as $F_{340/380}$ and were corrected for background fluorescence.

Surface electrocardiogram (ECG)

Mice were anesthetized using 2% isoflurane and supplemented with O_2 at 1.5 liters/min. A level plane of anesthesia was maintained at 1–2% isoflurane supplemented with O_2 at 1.5 liters/min. Mice were placed in prone position on a Mouse Monitor S (Indus Instruments) and recorded according to the manufacturer's recommended settings for 5 min under the default filter set. ECGs were recorded for leads I, II, III, and aVL for each animal and analyzed. For intrinsic heart rate, atropine (1 mg/kg) + propranolol (1 mg/kg) were administered intraperitoneally.

Echocardiography

Transthoracic echocardiography was performed using the Visual Sonics 3100 imaging system equipped with a 505s 40-MHz probe. Mice underwent transthoracic echocardiography under light anesthesia (inhaled isoflurane 1–2%) with heart rate (350–500 beats per minute) and core temperature (37°C) continuously monitored. The heart was visualized in 2-D form from modified parasternal long-axis, short-axis, and apical views. The left ventricular dimensions and calculated left ventricular ejection fraction were measured from the short-axis M-mode display. All measurements were obtained in triplicate and averaged. The sonographer was blinded to animal genotype, and data analysis was performed with animal genotype blinded. For the pharmacological stress echocardiogram, a single intraperitoneal injection of ISO (30 mg/kg, United States Pharmacopeia) was administered immediately after baseline echocardiographic measurements were recorded. Heart rate was monitored; within 5 min of increased heart rate, the drug effect was confirmed, and echocardiographic measures were repeated.

Quantitative reverse transciption PCR (qRT-PCR)

Mice were anesthetized with ketamine and xylazine, and their hearts were quickly excised, after which the apex of the left ventricle was removed and snap frozen in liquid nitrogen. Frozen tissue was then homogenized, and RNA was isolated using the Direct-zol RNA kit (Zymo Research) and quantified using a NanoDrop spectrophotometer (Thermo Fisher Scientific). cDNA was generated from 500 ng of RNA, which was then amplified via RT-PCR using TaqMan probes from Life Technologies: *gapdh* (Mm99999915_g1) and *rrad* (Mm00451053_m1). Cycle threshold (C_T) values for *rrad* were normalized by subtraction from *gapdh*, and WT was then subtracted from $RAD^{-/-}$ ($\Delta\Delta C_T$), and fold changes were calculated as $2^{-\Delta\Delta CT}$.

Statistical analysis

For statistical analyses performed on all cellular observations, the mouse is the primary unit of analysis. Cellular mean ± SEM values are represented in the figures. The within-mouse averages of the cellular observations were used for analysis to perform the analysis on the level of the experimental units, the mice. The factors of mouse type and voltage test (2 × 2 factorial design) were analyzed using two-way repeated-measures ANOVA, which was performed with Šídák's multiple comparisons test to compare CTRL versus cRadKO pairs at the same voltage step. In the analyses involving the difference of means between CTRL and cRadKO mice under the assumption of normality of response variable, two-sample unpaired *t* tests were used for CTRL versus cRadKO, and paired *t* tests were used for before-and-after ISO treatment comparisons. $P < 0.05$ was considered statistically significant. All statistical analyses were performed using GraphPad Prism 9. Sample sizes are reported as N = number of mice and n = number of cells. $P < 0.05$ was considered statistically significant. All statistical analyses were performed using GraphPad Prism 9.

Online supplemental material

Fig. S1 shows the effect of ISO on $I_{Ca,L}$ measured from CTRL ventricular cardiomyocytes. Fig. S2, Fig. S3, and Fig. S5 show the 95% confidence intervals of the two-way repeated-measures ANOVA tabular results for figure panels that show remaining current. Fig. S4 describes the surface ECG measurements for CTRL versus cRadKO at baseline (before and after treatment with atropine and propranolol). Fig. S6 shows characterization of the dKO and tKO mouse models (echocardiographic assessment, qRT-PCR, and ECG measurements).

Results

cRadKO mirrors modulated LTCC

$I_{Ca,L}$ decay consists of an early, fast component and a late, slow component (Pelzer et al., 1990; Mahajan et al., 2008; Madhvani

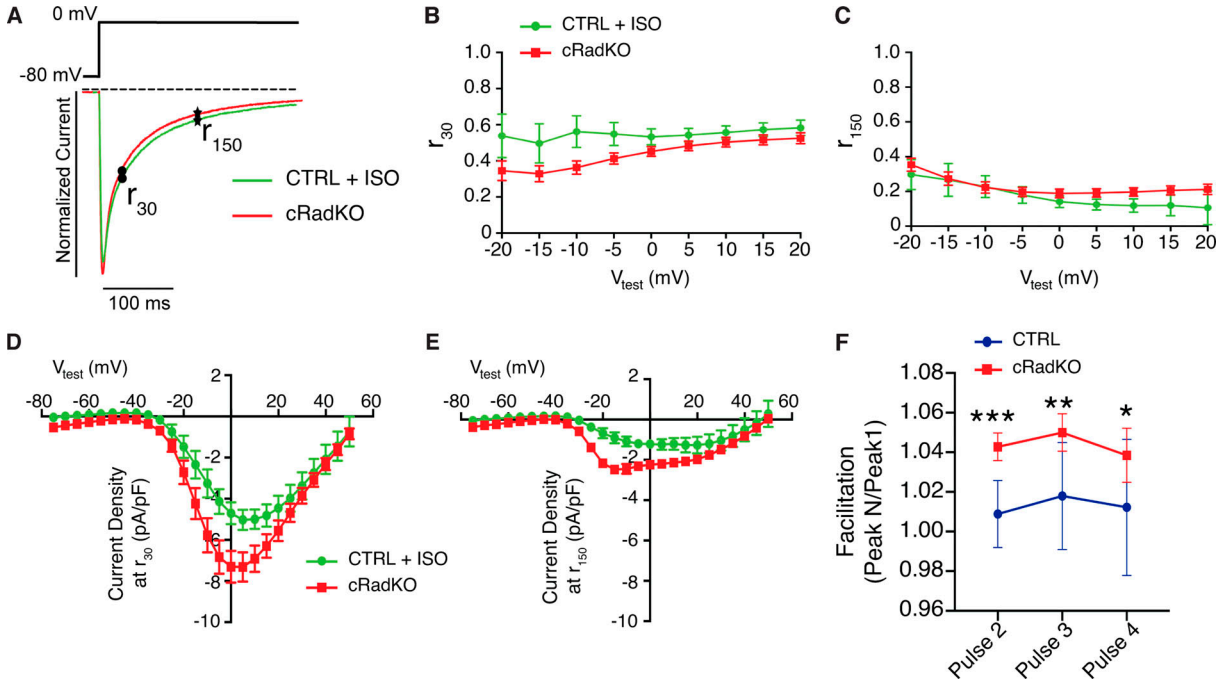

Figure 1. **Rad deletion $I_{Ca,L}$ phenocopies modulated $I_{Ca,L}$. (A)** Exemplar Ca^{2+} currents with 10 mM EGTA for CTRL with ISO (green) and cRadKO (no ISO; red). Traces are normalized to peak current at 0 mV. Scale bar, 100 ms. Black dots indicate r_{30}; black stars indicate r_{150}. **(B–E)** Remaining current across voltage steps 30 ms after peak (B) and 150 ms after peak (C). $I_{Ca,L}$ current density 30 ms (D) and 150 ms (E) after peak. Data in B and C were analyzed by two-way ANOVA plus Šídák's multiple comparisons test. *n* = 4 mice, *n* = 7 cells for CTRL; *n* = 10 mice, *n* = 23 cells for cRadKO. **(F)** Facilitation measured as peak current (without ISO) across multiple pulses of cells at 1 Hz normalized to the first pulse, then pooled, demonstrating significant increase in current across pulses in cRadKO (*, P = 0.03; **, P = 0.002; ***, P = 0.0008); there was no significant difference in current across pulses in CTRL. Data are presented as mean ± SEM values. Data in F were analyzed by one-sample *t* test compared with a hypothetical mean of 1. Data in F are displayed from *n* = 4 mice, 11 cells for CTRL; *n* = 4 mice, *n* = 7 cells for cRadKO.

et al., 2011; Karagueuzian et al., 2017; Madhvani et al., 2015). CDI is the dominant mechanism of inactivation of the fast component and under conditions of β-adrenergic stimulation (Peterson et al., 1999; Zamponi, 2003; Findlay, 2002a; Madhvani et al., 2011); this idea, coupled with the emergent model that phosphorylated Rad is reoriented from the LTCC during β-adrenergic stimulation to drive $I_{Ca,L}$ modulation (Ahern et al., 2019; Manning et al., 2013; Levitan et al., 2016; Liu et al., 2020), predicts that Rad deletion (in the basal state) should yield $I_{Ca,L}$ properties that are not different from those of WT (CTRL) following β-adrenergic modulation. We therefore compared the kinetics of $I_{Ca,L}$ in cardiomyocytes from CTRL after the addition of ISO with basal $I_{Ca,L}$ in cardiomyocytes from cRadKO (Fig. 1). For brevity, we henceforth refer to CTRL $I_{Ca,L}$ and cRadKO $I_{Ca,L}$ as stand-ins for $I_{Ca,L}$ from CTRL or cRadKO ventricular cardiomyocytes. EGTA was used to allow a readout of the influence on global Ca^{2+}. $I_{Ca,L}$ traces from cRadKO and ISO-stimulated CTRL normalized to peak current demonstrate that basal cRadKO $I_{Ca,L}$ decay is not different from that of modulated CTRL (Fig. 1 A). Remaining current 30 ms after peak (r_{30}) was not different between modulated CTRL $I_{Ca,L}$ and cRadKO $I_{Ca,L}$ (Fig. 1 B, Fig. S1, and Fig. S2 A for two-way ANOVA tabular results); similarly, there was no difference in the late component (remaining current 150 ms after peak [r_{150}]; Lacinová and Hofmann, 2005; Mahajan et al., 2008; Markandeya and Kamp, 2015; Madhvani et al., 2015) at individual voltage steps (Fig. 1 C and Fig. S2 B for two-way ANOVA tabular results). cRadKO displayed larger current density than CTRL at r_{30} (Fig. 1 E) and r_{150} (Fig. 1 F). Taken together, these results demonstrate that the kinetic signature of basal cRadKO approximates modulated $I_{Ca,L}$ kinetics.

Increased Ca^{2+} and Rad both contribute to CDI

If CDI is the dominant mechanism when the LTCC is modulated, then the source of calcium contributing to CDI could emanate from the SR or from local calcium entering through the channel itself (Grandi et al., 2010). To evaluate global versus local Ca^{2+}, we investigated $I_{Ca,L}$ decay kinetics in the presence of either EGTA or BAPTA. These calcium buffers have similar steady-state binding affinities for calcium, but they differ in binding rate constants (Naraghi and Neher, 1997). EGTA buffers slower than BAPTA and allows investigation of the influence of global calcium on CDI; by contrast, the use of BAPTA limits CDI to local sources, mainly Ca^{2+} fluxing in the nanodomain of the channel (Naraghi and Neher, 1997; Fakler and Adelman, 2008).

Fig. 2 summarizes the analysis of r_{30} between cRadKO $I_{Ca,L}$ and CTRL $I_{Ca,L}$ under conditions reporting global Ca^{2+} (EGTA used as calcium buffer). Traces from cRadKO and CTRL $I_{Ca,L}$ demonstrate that cRadKO $I_{Ca,L}$ fast decay is greater than that for CTRL (Fig. 2 A). Across multiple voltage steps, there is less r_{30} in cRadKO $I_{Ca,L}$ than in CTRL $I_{Ca,L}$ (Fig. 2 B and Fig. S2 C for two-way ANOVA tabular results). Current density was larger in

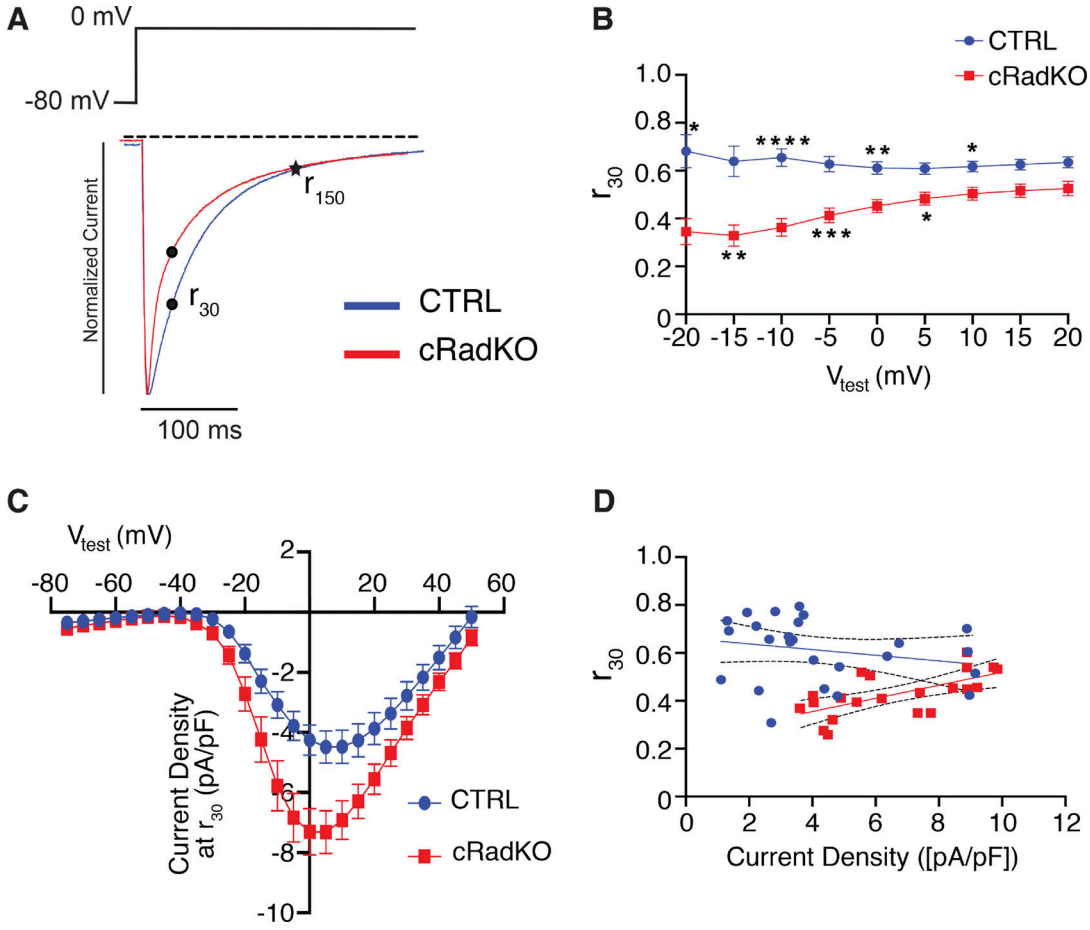

Figure 2. **Rad deletion accelerates fast component of $I_{Ca,L}$ decay. (A)** Exemplar Ca^{2+} currents with 10 mM EGTA for CTRL (blue) and cRadKO (red). Traces were normalized to peak current at 0 mV. Scale bar, 100 ms. Black dots indicate r_{30}. **(B)** Remaining current 30 ms after peak across voltage steps. **(C)** $I_{Ca,L}$ current density 30 ms after peak. **(D)** Regression plot of the absolute values of current density versus r_{30} (CTRL: slope = −0.01, deviation from zero: P = 0.28, r^2 = 0.5; cRadKO: slope = 0.03, deviation from zero: P = 0.002, r^2 = 0.4; dotted lines represent 95% confidence intervals). Data in B and C are presented as mean ± SEM values. Data in B were analyzed by two-way ANOVA plus Šídák's multiple comparisons test (for between CTRL and cRadKO: *, P < 0.05; **, P < 0.01; ***, P < 0.001; and ****, P < 0.0001, alternating asterisks for presentation clarity). Data in D were analyzed by simple linear regression. *n* = 10 mice, *n* = 25 cells for CTRL; *n* = 10 mice, *n* = 23 cells for cRadKO.

cRadKO than in CTRL (Fig. 2 C). To assess whether remaining current depended on elevated current density, we plotted r_{30} as a function of current density (Fig. 2 D). CTRL trends toward a negative slope, meaning that as current density increases, there is less remaining current, as expected for early, fast inactivation by CDI (Findlay, 2004). In contrast, cRadKO has a positive slope; as current density increases, there is more remaining current. This finding suggests a Ca^{2+}-independent contribution to the early, fast component of decay in a Rad-less LTCC.

We next assessed r_{30} in the presence of BAPTA to limit the pool of calcium local to the channel complex (Naraghi and Neher, 1997; Fakler and Adelman, 2008; Fig. 3). Representative traces reveal an apparent smaller difference in decay between cRadKO and CTRL (Fig. 3 A). r_{30} across individual test potentials demonstrates no significant difference between cRadKO and CTRL $I_{Ca,L}$ (Fig. 3 B and Fig. S2 D for two-way ANOVA tabular results). In the presence of BAPTA, cRadKO maintains a larger current density than CTRL (Fig. 3 C). Local buffering by BAPTA eliminates the negative correlation of r30 with current density for CTRL $I_{Ca,L}$; however, the positive correlation of cRadKO r30 and current density remains in the presence of BAPTA (Fig. 3 D; compare with Fig. 2 D). Taken together, these results suggest that the early, fast decay of $I_{Ca,L}$ in cRadKO is driven in part by SR released calcium and in part by a Ca^{2+}-independent mechanism.

Calcium released from the SR contributes to CDI (Morotti et al., 2012). Thus, enhanced CDI seen in cRadKO could be the result of a larger calcium release from the SR in response to larger $I_{Ca,L}$ current density, enhanced calcium cycling, and increased SERCA expression (Ahern et al., 2019). We therefore measured SR calcium content as caffeine-induced calcium transients (Fig. 4). Representative calcium transients followed by caffeine application (Fig. 4 A) demonstrate a greater twitch (Fig. 4 B; **, P = 0.004) and greater SR calcium content in cRadKO than in CTRL (Fig. 4 C; *, P = 0.02). The fractional change in amplitude between twitch calcium versus caffeine-released calcium was greater in cRadKO, demonstrating that there is more calcium released from the SR beat to beat

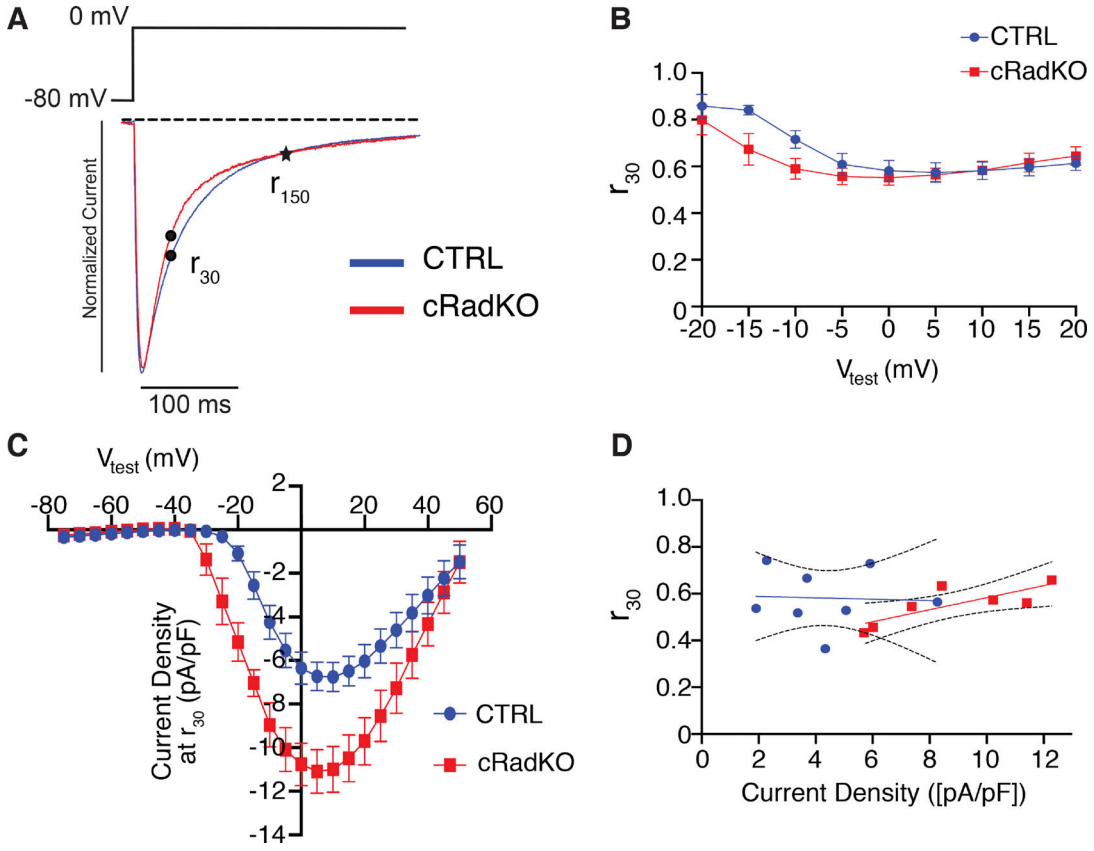

Figure 3. **Rad regulation of $I_{Ca,L}$ kinetics requires SR Ca^{2+} release. (A)** Exemplar Ca^{2+} currents with 10 mM BAPTA for CTRL (blue) and cRadKO (red). Traces were normalized to peak current at 0 mV. Scale bar, 100 ms. Black dots indicate r_{30}. **(B)** Remaining current 30 ms after peak across voltage steps. **(C)** $I_{Ca,L}$ current density 30 ms after peak. **(D)** Regression plot of the absolute values of current density versus r_{30} (CTRL: slope = −0.003, deviation from zero: P = 0.91, r^2 = 0.002; cRadKO: slope = 0.03, deviation from zero: P = 0.03, r^2 = 0.6; dotted lines represent 95% confidence intervals). Data in B and C are presented as mean ± SEM values. Data in B were analyzed by two-way ANOVA plus Šídák's multiple comparisons test. Data in D were analyzed by simple linear regression. *n* = 4 mice, *n* = 8 cells for CTRL; *n* = 4 mice, *n* = 7 cells for cRadKO.

(Fig. 4 D). There was no significant difference in the rate of decay of the caffeine-induced calcium transient, indicating no difference in Na^+/Ca^{2+} exchanger activity in cRadKO compared with CTRL (Fig. 4 E). Taken together, these results are consistent with a contribution of greater calcium release from the SR accelerating CDI in cRadKO.

The absence of Rad does not promote pathological alterations to late $I_{Ca,L}$ kinetics

Late $I_{Ca,L}$ contributes to repolarization and SR calcium loading (Mahajan et al., 2008); impaired inactivation of the late phase can result in APD prolongation and early afterdepolarizations (EADs; Mahajan et al., 2008; Markandeya and Kamp, 2015; Madhvani et al., 2011; Karagueuzian et al., 2017; Madhvani et al., 2015). We therefore analyzed $I_{Ca,L}$ r_{150} in cRadKO and CTRL in the presence of EGTA. Representative traces demonstrate no difference between cRadKO and CTRL $I_{Ca,L}$ (Fig. 2 A, superimposed star). There was no difference in r_{150} between the models at multiple test potentials (Fig. 5 A and Fig. S2 E for two-way ANOVA tabular results). cRadKO, compared with CTRL, has larger current density at r_{150} (Fig. 5 B). A positive correlation is seen in both cRadKO and CTRL when r_{150} is displayed as a function of current density (Fig. 5 C). In the presence of BAPTA, there was no difference in r_{150} (see Fig. 3 A, overlapping stars at r_{150}; Fig. 5 D; and Fig. S2 F for two-way ANOVA tabular results). Current density was not different for cRadKO compared with CTRL $I_{Ca,L}$ (Fig. 5 E). r_{150} plotted against current density demonstrated a positive correlation in both cRadKO and CTRL (Fig. 5 F). These data show that Rad deletion does not promote alterations to late $I_{Ca,L}$ kinetics.

The late, slow component of $I_{Ca,L}$ decay is thought to be dominated by VDI (Findlay, 2002a; Findlay, 2004; Morales et al., 2019). We therefore measured VDI in cRadKO by using barium as the charge carrier (Fig. 6). Representative traces demonstrate faster decay in cRadKO than in CTRL at both r_{30} and r_{150} (Fig. 6 A). There was less r_{30} in cRadKO (Fig. 6, B and D; Fig. S3 A reports two-way ANOVA tabular results for Fig. 6 B). At r_{150}, remaining current in cRadKO was not significantly less than that in CTRL (Fig. 6, C and E; Fig. S3 B reports two-way ANOVA tabular results for Fig. 6 C). A positive correlation is seen in cRadKO when either r_{30} or r_{150} is plotted as a function of current density (Fig. 6, F and G). These data, in concert with the regression plots from Figs. 2 and 3, show that the absence of Rad enhances VDI. This suggests that the presence of Rad contributes to dampening VDI.

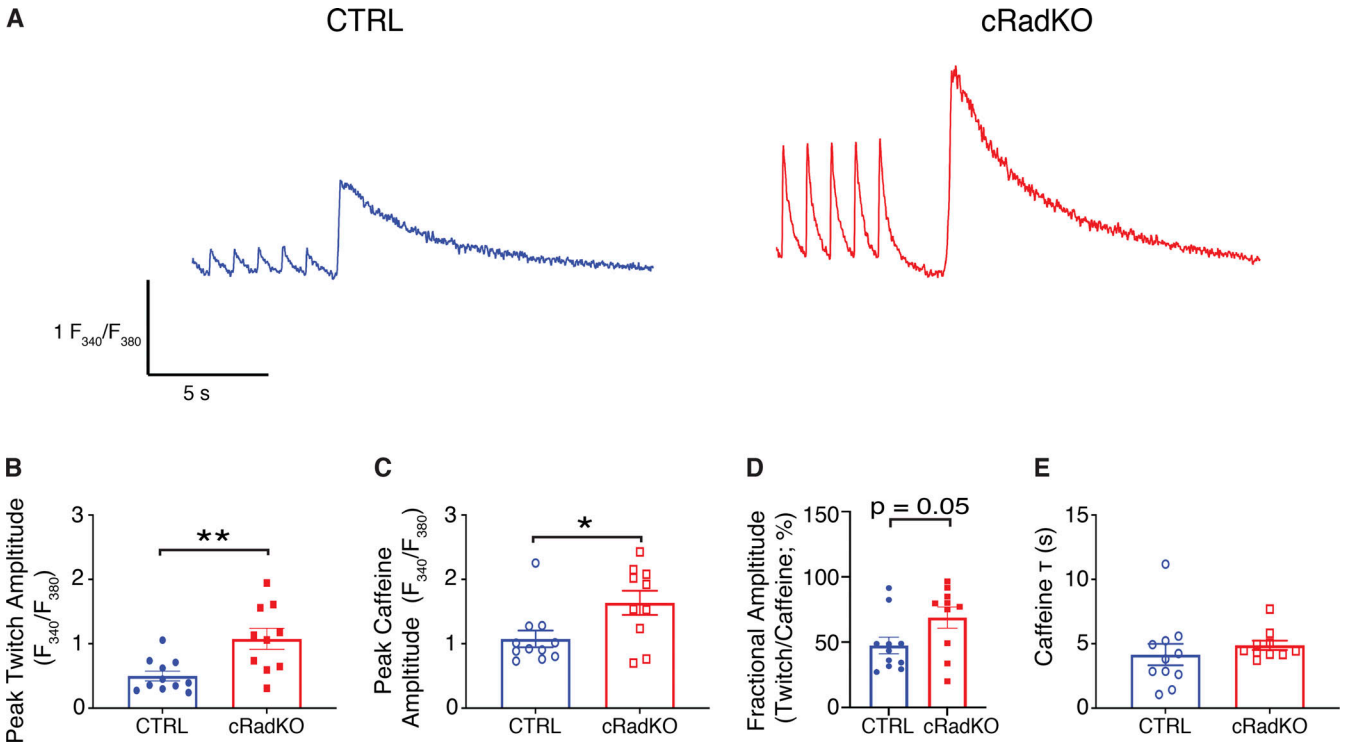

Figure 4. **Rad deletion displays larger SR calcium content. (A)** Representative transients before and after administration of 10 mM caffeine. CTRL in blue and cRadKO in red. **(B)** Peak twitch amplitude (**, P = 0.004). **(C)** Peak caffeine amplitude (*, P = 0.02). **(D)** Fractional amplitude between twitch and caffeine (P = 0.05). **(E)** Rate of decay of caffeine transient (P = 0.45). CTRL: *n* = 6 mice, *n* = 11 cells; cRadKO: *n* = 4 mice, *n* = 10 cells. Data in B–E are presented as mean ± SEM values. P values were calculated using Student's unpaired *t* test for B–E.

Faster kinetics in cRadKO prevent alterations to cardiac electrophysiology

$I_{Ca,L}$ plays a critical role in regulating cardiac APD; slight alterations to current density or inactivation of the LTCC can lead to electrical dysfunction, such as AP prolongation, EADs, and prolonged QT intervals (Splawski et al., 2004; Splawski et al., 2005; Mahajan et al., 2008; Markandeya and Kamp, 2015; Madhvani et al., 2011; Karagueuzian et al., 2017; Madhvani et al., 2015). Sympathetic stimulation via the β-AR signaling axis modulates triggered calcium and shortens APD (Shen and Zipes, 2014). Studies have shown that female mice exhibit prolonged AP repolarization and longer QT intervals (Bayer et al., 2001), making females more sensitive to revealing if Rad deletion has an effect on APD and QT interval. We therefore measured APs from isolated ventricular cardiomyocytes and used surface ECG recordings to assess the QT interval in female mice. APs measured at 1 Hz from CTRL ventricular cardiomyocytes showed a pronounced inflection point positive to 0 mV (Fig. 7 A, arrow), rapid repolarization, and a slower repolarization phase negative to −50 mV (Fig. 7 A). cRadKO APs (Fig. 7 A, red line) demonstrated similar morphology to CTRL at baseline (Fig. 7 A, blue line) and after addition of ISO (Wang et al., 2019; Fig. 7 B; cRadKO, black line; CTRL, green line). Baseline AP amplitudes were not significantly different between models (Fig. 7 C; cRadKO, 127.4 ± 1.0 mV; CTRL, 123.0 ± 3.3 mV). Comparison of baseline APD at 50% repolarization (APD_{50}) and at 80% repolarization (APD_{80}) demonstrated no significant difference between cRadKO and CTRL (Fig. 7 D; cRadKO, 6.5 ± 0.98 ms; CTRL, 6.2 ± 0.58 ms). At APD_{80}, cRadKO demonstrated faster repolarization than CTRL (Fig. 7 E; cRadKO, 17.1 ± 1.5 ms; CTRL, 21.2 ± 1.1 ms). CTRL AP amplitude was not significantly different from cRadKO after ISO (Fig. 7 F). cRadKO at APD_{50} was slightly shorter than at baseline but was not significantly different from CTRL (Fig. 7 G; APD_{50} after ISO, cRadKO, 6.4 ± 1.2 ms; CTRL, 6.0 ± 0.71 ms). CTRL was longer at APD_{80} than at baseline but was not significantly different from cRadKO (Fig. 7 H; APD_{80} after ISO, cRadKO, 18.0 ± 1.8 ms; CTRL, 23.4 ± 2.0 ms).

We next assessed in vivo electrical function. The increase in heart rate in response to sympathetic stimulation is the result of integrative mechanisms in both branches of the autonomic nervous system (Shen and Zipes, 2014), which could obscure a potential effect on QT interval due to a selective increase in $I_{Ca,L}$ in the absence of Rad. We therefore measured the ECG under autonomic nervous system block by treating the mice with atropine and propranolol (Wickman et al., 1998). Baseline ECG measurements demonstrated no significant difference in QT or corrected QT interval (QTc; Fig. S4). After administration of atropine and propranolol, representative surface ECG traces showed no apparent differences between CTRL and cRadKO (Fig. 7 I). Raw QT interval (Fig. 7 J; cRadKO, 40 ± 6 ms; CTRL, 50 ± 7 ms; P = 0.35) and QTc demonstrated no significant difference (Fig. 7 K; cRadKO, 33 ± 5 ms; CTRL, 40 ± 5 ms; P = 0.41). These data, combined with the AP measurements, support the idea that the faster kinetics balance the increase in peak $I_{Ca,L}$, thereby preventing significant alterations in cardiac electrophysiology.

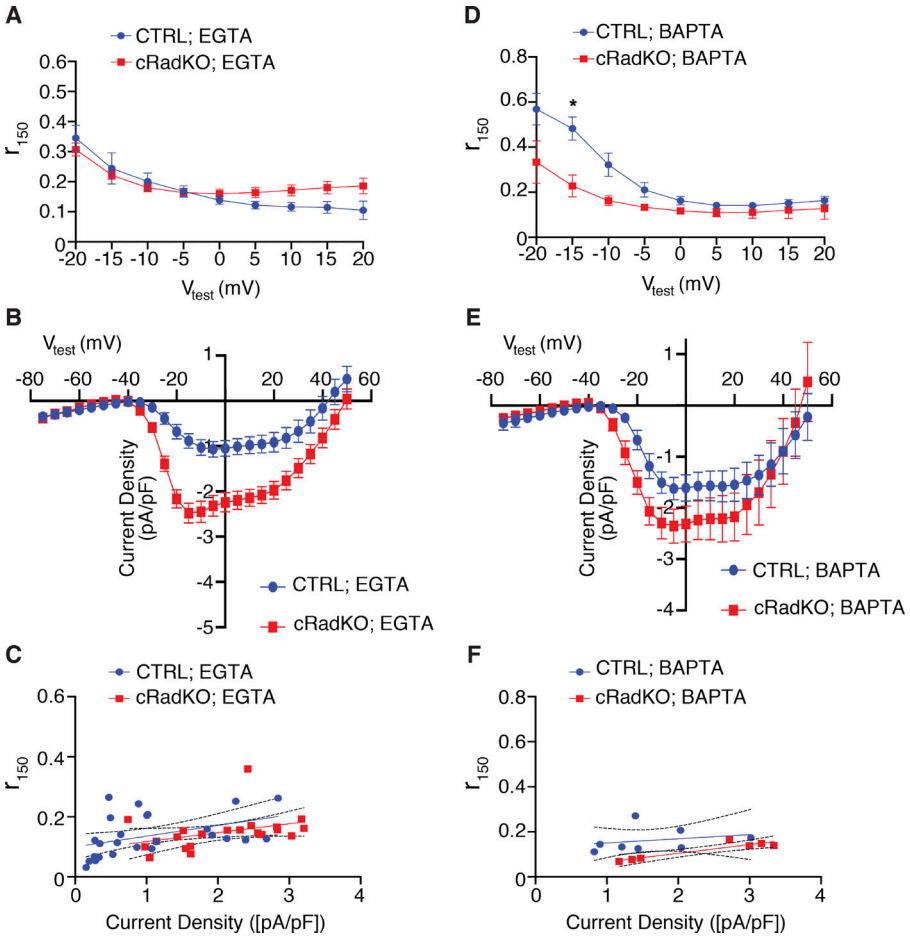

Figure 5. **The absence of Rad does not promote pathological alterations to late $I_{Ca,L}$ kinetics. (A–C)** Current measured with EGTA. **(D–F)** Current measured with BAPTA. **(A)** Remaining current 150 ms after peak across voltage steps. **(B)** $I_{Ca,L}$ current density 150 ms after peak. **(C)** Regression plot of the absolute values of current density versus r_{150} (CTRL: slope = 0.04, deviation from zero: P = 0.03, r^2 = 0.2; cRadKO: slope = 0.03, deviation from zero: P = 0.09, r^2 = 0.2; dotted lines represent 95% confidence intervals). *n* = 10 mice, *n* = 25 cells for CTRL; *n* = 10 mice, *n* = 23 cells for cRadKO. **(D)** Remaining current 150 ms after peak across voltage steps. **(E)** $I_{Ca,L}$ current density 150 ms after peak. **(F)** Regression plot of the absolute values of current density versus r_{150} (CTRL: slope = 0.02, deviation from zero: P = 0.54, r^2 = 0.1; cRadKO: slope = 0.04, deviation from zero: P = 0.003, r^2 = 0.9; dotted lines represent 95% confidence intervals). *n* = 4 mice, *n* = 8 cells for CTRL; *n* = 4 mice, *n* = 7 cells for cRadKO. Data in A, B, D, and E are presented as mean ± SEM values. Data in A and D analyzed by two-way ANOVA plus Šídák's multiple comparisons test. For between CTRL and cRadKO: *, P = 0.03. Data in C and F were analyzed by simple linear regression.

cRadKO yields modulated kinetics of LTCC downstream of β-AR signaling

It is possible that tonic PKA activity is involved in the increase in $I_{Ca,L}$ current density and hyperpolarized shift in activation that are seen in cRadKO (Bryant et al., 2014; Bryant et al., 2018). We therefore assessed $I_{Ca,L}$ in cRadKO and CTRL following exposure to 2 µM H89. However, in the presence of PKA inhibition, cRadKO retained a modulated $I_{Ca,L}$ phenotype. Peak $I_{Ca,L}$ was significantly increased in cRadKO compared with CTRL (Fig. 8 A). Rad deletion also resulted in a greater maximal conductance (Fig. 8 B; Gmax, cRadKO, 386 ± 49 pS/pF; CTRL, 224 ± 33 pS/pF; P = 0.03) and a negative shift in activation midpoint (Fig. 8, C and D; cRadKO, 0.18 ± 1.6 mV; CTRL, 6.7 ± 3.0 mV; P = 0.04). Analysis of kinetics demonstrated a trend of less remaining current in cRadKO at r_{30} and r_{150} (Fig. 8, E and F; Fig. S5, A and B report two-way ANOVA tabular results for Fig. 8, E and F, respectively). Taken together, these results support the hypothesis that the deletion of Rad increases peak $I_{Ca,L}$ that mirrors modulated LTCCs without activation of PKA.

β_1-AR activation mediates positive chronotropic and inotropic responses of cardiomyocytes, and β_2-AR is thought to contribute to these processes more locally within cardiomyocytes (Nikolaev et al., 2010). To determine whether these receptors were contributing to the modulation effect of $I_{Ca,L}$ seen in cRadKO, we bred $RAD^{fl/fl\text{-}MHC\text{-}MCM}$ onto a β_1,β_2-AR dKO mouse (Chruscinski et al., 1999) to create an induced $RAD^{\Delta/\Delta},\beta_1,\beta_2$-AR tKO mouse after administration of tamoxifen. Echocardiographic assessment of dKO and tKO compared with CTRL demonstrated elevated cardiac function in tKO but no significant difference in dKO (Fig. S6). Ejection fraction was significantly different between CTRL and dKO after acute ISO, demonstrating that β_1,β_2-AR response was disrupted (Fig. S6 E; CTRL, 93 ± 1%, dKO, 60 ± 3%; P < 0.0001; data for CTRL + ISO echocardiography taken from our previously published dataset; Ahern et al., 2019). Disruption of Rad expression in the heart in tKO was confirmed by qRT-PCR (Fig. S6 F). After the deletion of Rad, ejection fraction significantly increased in the tKO compared with dKO (Fig. 9, A and B; tKO, 72 ± 2%; dKO, 51 ± 4%; P < 0.0001). Left ventricular inner dimensions decreased in the tKO (Fig. 9 C; tKO, 3.6 ± 0.1 mm; dKO, 4.2 ± 0.1 mm; P = 0.003) without significant changes in the anterior or posterior walls (Fig. 9, D and E; for 9 D, tKO, 0.88 ± 0.1 mm; dKO, 0.80 ± 0.1 mm; P = 0.43; for 9 E, tKO, 0.86 ± 0.05 mm; dKO, 0.82 ± 0.1 mm; P = 0.52). Surface ECG showed no significant difference in raw QT interval (Fig. 9, F and G; tKO, 39 ± 4 ms; dKO, 30 ± 6 ms; P = 0.19), QTc (Fig. 9 H; tKO, 31 ± 4 ms; dKO, 23 ± 4 ms; P = 0.14), or RR interval (Fig. 9 I; tKO, 31 ± 4 ms; dKO, 23 ± 4 ms; P = 0.14) between dKO and tKO female mice. These data support that the absence of Rad enhances cardiac function independent of β_1,β_2-AR signaling.

At the level of channel current, peak $I_{Ca,L}$ was significantly increased in tKO compared with dKO (Fig. 10, A and B). Rad deletion also resulted in a greater maximal conductance (Fig. 10, C and D; Gmax, tKO, 508 ± 33 pS/pF; dKO, 230 ± 32 pS/pF;

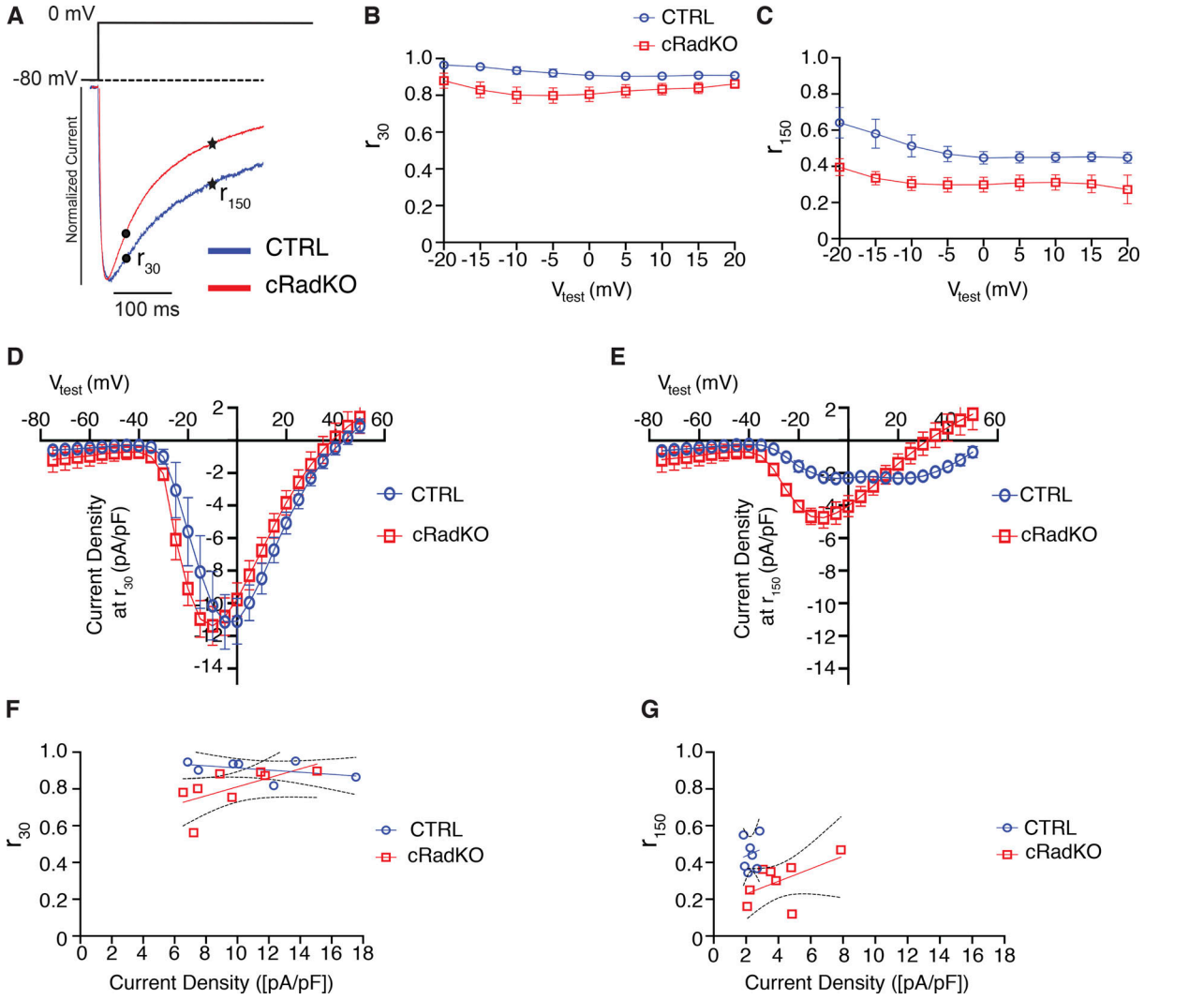

Figure 6. **Rad deletion enhances VDI. (A)** Exemplar Ca^{2+} currents with 10 mM EGTA for CTRL (blue) and cRadKO (red). Traces were normalized to peak current at 0 mV. Scale bar, 100 ms. Black dots indicate r_{30}. Black stars indicate r_{150}. **(B)** Remaining current 30 ms after peak across voltage steps. **(C)** Remaining current 150 ms after peak across voltage steps. **(D)** $I_{Ca,L}$ current density 30 ms after peak. **(E)** $I_{Ca,L}$ current density 150 ms after peak. **(F)** Regression plot of the absolute values of current density versus r_{30} (CTRL: slope = −0.006, deviation from zero: P = 0.33, r^2 = 0.2; cRadKO: slope = 0.02, deviation from zero: P = 0.10, r^2 = 0.4; dotted lines represent 95% confidence intervals). **(G)** Regression plot of the absolute values of current density versus r_{150} (CTRL: slope = 0.04, deviation from zero: P = 0.73, r^2 = 0.03; cRadKO: slope = 0.03, deviation from zero: P = 0.16, r^2 = 0.3; dotted lines represent 95% confidence intervals). *n* = 3 mice, *n* = 7 cells for CTRL; *n* = 4 mice, *n* = 8 cells for cRadKO. Data in B–E are presented as mean ± SEM values. Data in A and D were analyzed by two-way ANOVA plus Šídák's multiple comparisons test. Data in C and F were analyzed by simple linear regression.

P < 0.0001) and a negative shift in activation midpoint (Fig. 10 E; tKO, −13.1 ± 2.4 mV; dKO, −6.12 ± 1.7 mV; P = 0.04). Analysis of kinetics demonstrated a trend of less remaining current in the tKO at r_{30} (Fig. 10, F, G, and I) and no difference at r_{150} (Fig. 10, F, H, and J). The interaction of voltage and dKO versus tKO was significantly different both at r_{30} and r_{150} (Fig. S3, C and D). Taken together, these results support the hypothesis that the deletion of Rad increases peak $I_{Ca,L}$ that mirrors modulated LTCCs without stimulation of β_1,β_2-AR signaling.

Discussion

The main findings of this study are that in the absence of Rad, increased peak $I_{Ca,L}$ is balanced by accelerated CDI and VDI (Fig. 11). Accelerated LTCC kinetics prevent significant AP and QT interval prolongation. In fact, APD_{80} is shorter in cRadKO (Fig. 7). The loss of Rad from the LTCC complex results in modulated $I_{Ca,L}$ independent of β-AR signaling. To our knowledge, the cardiomyocyte-restricted Rad deletion model is the only known model to increase $I_{Ca,L}$ without disrupting calcium homeostasis and without promoting pathological signaling (Muth et al., 1999; Chen et al., 2011). Therefore, myocardial Rad–LTCC interaction is a potential therapeutic target for positive inotropy while preserving β-AR signaling cascades beyond the LTCC.

Rad contributes to regulation of LTCC inactivation

A major implication of this study is that the presence of Rad slows inactivation of the LTCC. The deletion of Rad accelerated

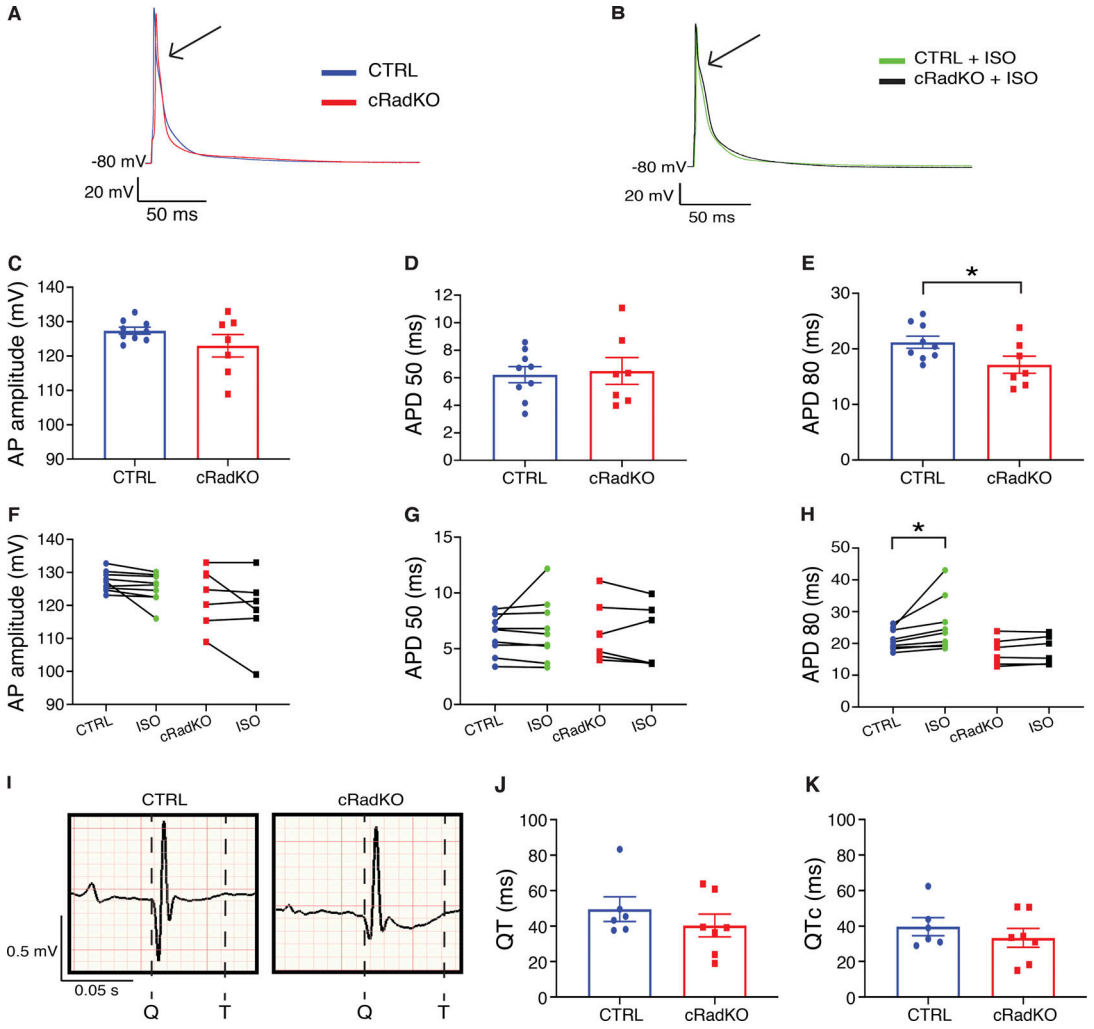

Figure 7. **Rad deletion does not prolong APD or QT interval. (A and B)** Exemplar APs (A) at baseline from CTRL (blue) and cRadKO (red) and (B) after ISO from CTRL (green) and cRadKO (black). Scale bars, 20 mV, 50 ms; arrows indicate the inflection point. **(C)** AP amplitude at baseline (P = 0.18). **(D)** APD_{50} at baseline (P = 0.81). **(E)** APD_{80} at baseline (*, P = 0.04). *n* = 2 mice, *n* = 9 cells for CTRL; *n* = 2 mice, *n* = 7 cells for cRadKO. **(F)** AP amplitude after ISO (CTRL: P = 0.10, cRadKO: P = 0.20). **(G)** APD_{50} after ISO (CTRL: P = 0.45; cRadKO: P = 0.38). **(H)** APD_{80} after ISO (CTRL: *, P = 0.05; cRadKO: P = 0.18). *n* = 2 mice, *n* = 9 cells for CTRL with ISO; *n* = 2 mice, *n* = 6 cells for cRadKO. **(I)** Representative raw QT interval of intrinsic heart rate from surface ECG of CTRL and cRadKO. Scale bar, 0.5 mV, 50 ms. **(J)** Raw QT interval (ms) is not significantly different (P = 0.35). **(K)** QTc (ms) is not significantly different (P = 0.41). CTRL: *n* = 6 mice; cRadKO: *n* = 7 mice. P values were calculated using Student's unpaired *t* test comparing CTRL with cRadKO (C–E, F–H, and J and K) and Student's paired *t* test comparing baseline with ISO (F–H). I and J were measured after administration of atropine (1 mg/kg) and propranolol (1 mg/kg). Data in C–E, J, and K are presented as mean ± SEM values.

only the early, fast component of $I_{Ca,L}$ decay without significantly altering the late, proarrhythmogenic component (Mahajan et al., 2008; Madhvani et al., 2011; Karagueuzian et al., 2017; Madhvani et al., 2015; Markandeya and Kamp, 2015; Figs. 1, 2, 3, 4, 5, and 6). Late $I_{Ca,L}$ has been implicated as a source of EADs; in many cardiac pathological conditions that are a high risk for ventricular tachycardia or ventricular fibrillation, the rate of $I_{Ca,L}$ inactivation can be slowed significantly, thereby generating an increase in late inward depolarizing current (Madhvani et al., 2011; Karagueuzian et al., 2017; Madhvani et al., 2015). This creates a pool of LTCCs that never inactivate (Madhvani et al., 2011; Karagueuzian et al., 2017; Madhvani et al., 2015). Three possibilities to treat EADs are (1) shifting $I_{Ca,L}$ steady-state activation in the depolarizing direction by <5 mV, (2) shifting steady-state inactivation in the hyperpolarizing direction by <5 mV, and (3) reducing the noninactivating component (Karagueuzian et al., 2017). The crucial aspect is to adjust the kinetics of $I_{Ca,L}$ to reduce window current without reducing peak $I_{Ca,L}$; this is a major downfall of traditional treatments such as verapamil or nifedipine (Karagueuzian et al., 2017). Indeed, reducing peak $I_{Ca,L}$ is not needed to suppress EAD formation, but rather only to decrease the late, arrhythmogenic component of $I_{Ca,L}$ (Karagueuzian et al., 2017; Madhvani et al., 2015). This way, excitation–contraction coupling and overall contractility are unaffected. One drug of promise that seems to decrease the late $I_{Ca,L}$ without affecting peak $I_{Ca,L}$ is roscovitine, a cyclin-dependent kinase inhibitor that is part of a new class of drugs known as "gate modifiers" (Karagueuzian et al., 2017, Madhvani et al., 2015; Han et al., 2019; Sheng et al., 2012; Yarotskyy and

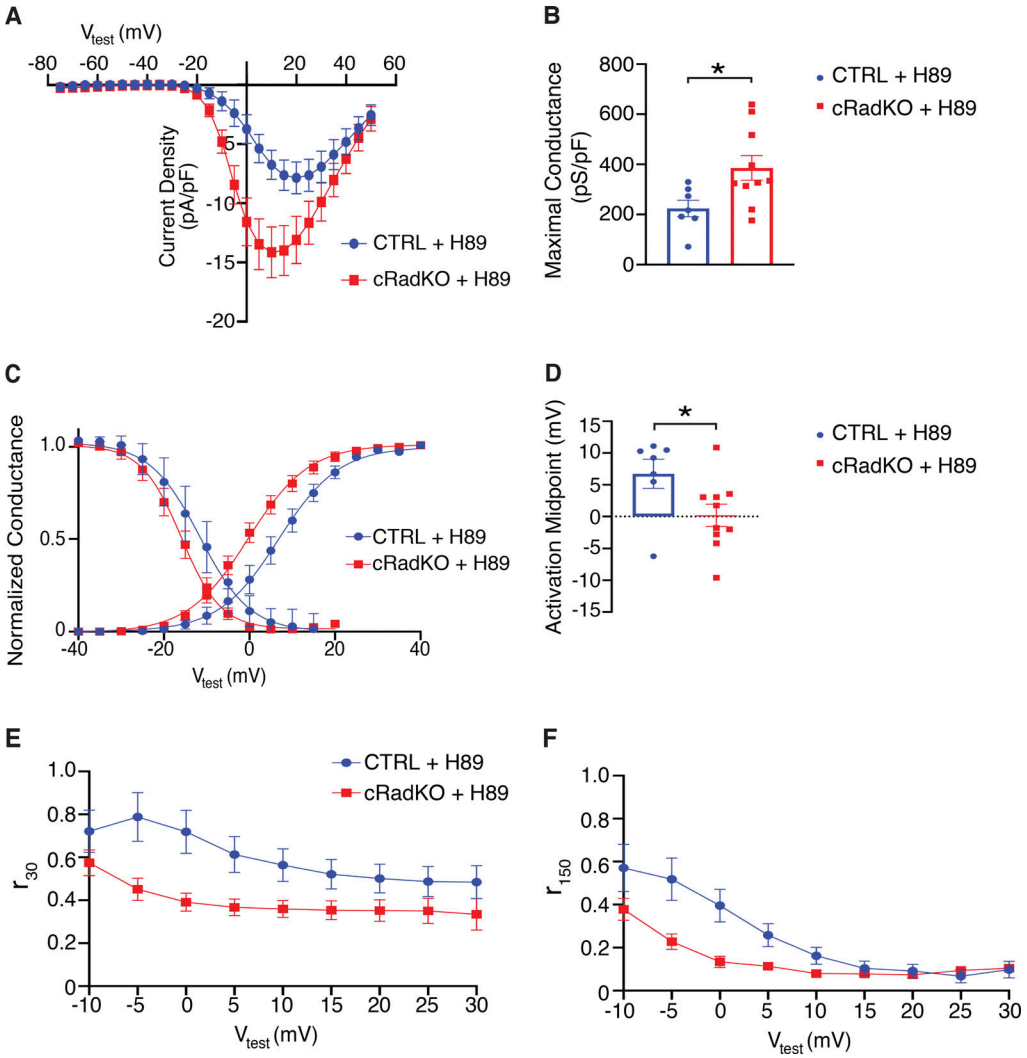

Figure 8. **Rad deletion yields modulated $I_{Ca,L}$ in the presence of PKA inhibition. (A)** Peak $I_{Ca,L}$ measured from isolated ventricular cardiomyocytes incubated in 2 µM H89 demonstrates larger current density in cRadKO than CTRL. **(B)** Maximal conductance is significantly larger in cRadKO than in CTRL in the presence of H89 (*, P = 0.03). **(C)** Conductance transform of I-V curve normalized to maximal conductance demonstrates a negative shift in activation in cRadKO compared with CTRL. Smooth curves are Boltzmann distributions fitted to data. **(D)** Activation midpoint is significantly negatively shifted in cRadKO compared with CTRL in the presence of H89 (*, P = 0.04). **(E)** Remaining current across voltage steps 30 ms after peak. **(F)** Remaining current across voltage steps 150 ms after peak. CTRL: *n* = 3 mice, *n* = 7 cells; cRadKO: *n* = 3 mice, *n* = 10 cells. P values calculated using Student's unpaired *t* test for C and D. Data are presented as mean ± SEM values. Data in E and F were analyzed by two-way ANOVA plus Šídák's multiple comparisons test.

Elmslie, 2007; Yarotskyy et al., 2009; Yazawa et al., 2011). It is possible that Rad is an endogenous gate modifier for the LTCC and that its removal selectively increases peak $I_{Ca,L}$ without increasing the late component. The absence of Rad illustrates a similar effect on window current compared with roscovitine in that there is a hyperpolarized shift in activation without an increase in pedestal current (Ahern et al., 2019; Manning et al., 2013). Further studies into how Rad specifically regulates the LTCC may contribute to the new class of gate-modifying drugs and how these mechanisms can be targeted to improve traditional treatments that use calcium channel block.

Rad is a key contributor to LTCC modulation

The activation of PKA downstream of β-AR stimulation results in an increase in $I_{Ca,L}$, an increase in channel open probability, and an increase in the number of functional channels (Bean et al., 1984; Ahern and Satin, 2019), also known as "modulation" of the LTCC. Phosphorylation of $Ca_V1.2$ was long thought to be the underlying mechanism of modulation (Pallien and Klussmann, 2020), but recent studies have proposed that the mechanism of modulation relies more on protein–protein interactions within the LTCC or on LTCC clustering (Pallien and Klussmann, 2020; Ahern et al., 2019; Liu et al., 2020; Navedo et al., 2010; Dixon et al., 2012; Dixon et al., 2015; Ito et al., 2019; Ahern and Satin, 2019). It was also recently shown that Rad is essential for cAMP-PKA regulation of $Ca_V1.2$ (Liu et al., 2020). Our studies have demonstrated that Rad–LTCC interaction is a key molecular signaling axis for LTCC modulation, both in the ventricle and in sinoatrial node cardiomyocytes (Ahern et al., 2019; Ahern, unpublished data), and that the absence of Rad

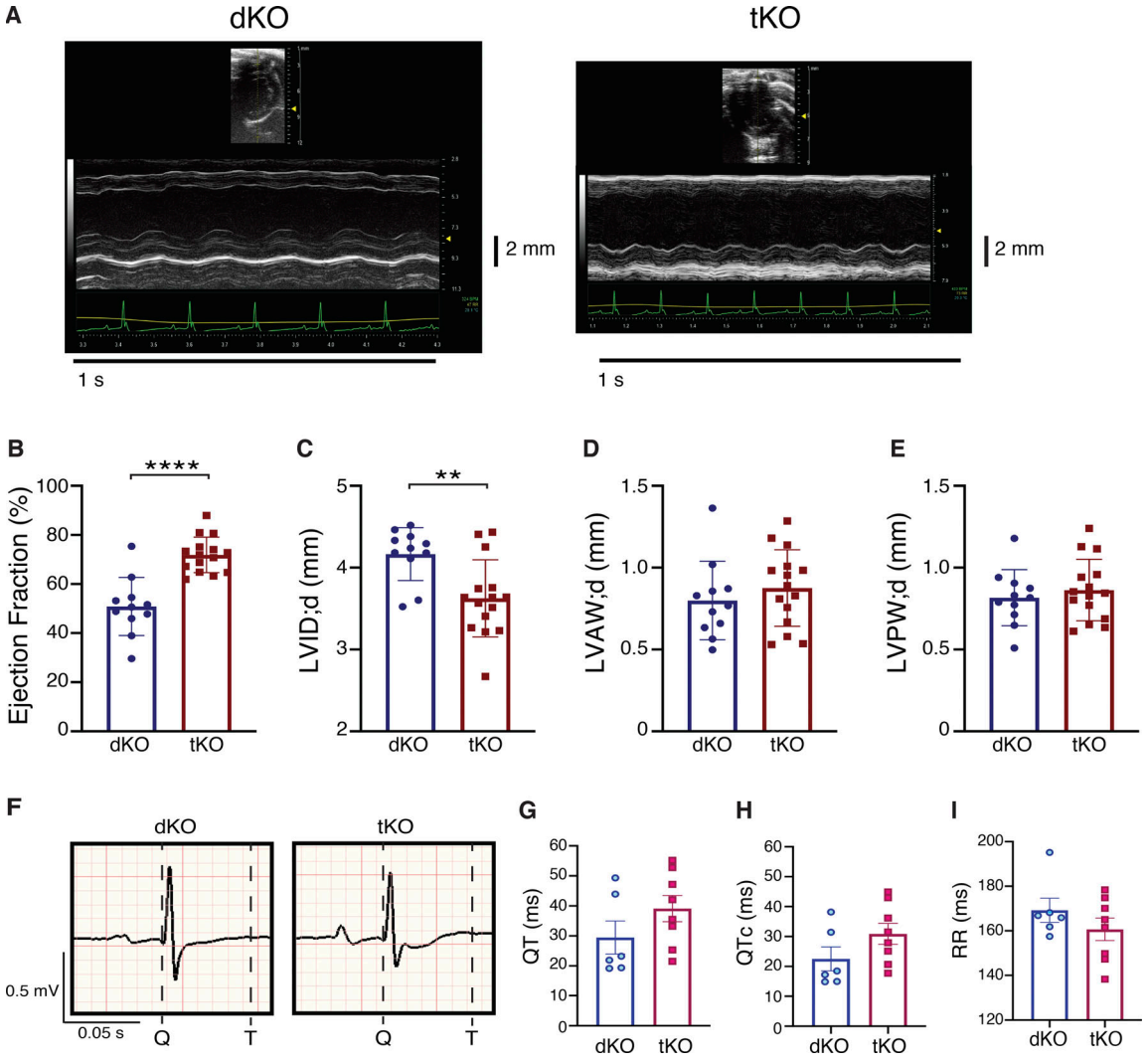

Figure 9. **Rad deletion increases heart function exclusive of $\beta_1\beta_2$-ARs. (A)** Representative M-mode short-axis echocardiography from dKO and tKO mice. Scale bars, 1 s; 2 mm. **(B)** Ejection fraction (****, P < 0.0001). **(C)** Left ventricular inner dimensions; diastole (LVID;d; **, P = 0.003). **(D and E)** Left ventricular anterior wall; diastole (LVAW;d; P = 0.43; D) and left ventricular posterior wall; diastole (LVPW;d; P = 0.52; E) thickness. Dimensions in C–E were measured in diastole. dKO: *n* = 11 mice; tKO: *n* = 15 mice. **(F)** Representative raw QT interval from surface ECG of dKO and tKO. Scale bar, 0.5 mV, 50 ms. **(G)** Raw QT interval (ms) is not significantly different (P = 0.19). **(H)** QTc (ms) is not significantly different (P = 0.14). **(I)** R-R interval (ms) is not significantly different (P = 0.27). dKO: *n* = 6 mice; tKO: *n* = 8 mice. P values were calculated using Student's unpaired *t* test for B–E and G–I. Data in B–E and G–I are presented as mean ± SEM values.

from the complex yields modulation of the LTCC. Our current findings expand on this through kinetic analysis, demonstrating that CTRL $I_{Ca,L}$ stimulated with ISO decayed in a manner that was indistinguishable from cRadKO $I_{Ca,L}$ (Fig. 1). When treated with ISO, channels may form "superclusters" along the t-tubules to amplify Ca^{2+} influx (Ito et al., 2019) and modify kinetics. The absence of Rad could promote these superclusters to form under basal conditions, which could in turn promote more CICR from the SR to feed back into the clusters to then accelerate CDI. The superclusters that form in response to sympathetic stimulation via the β-AR axis signaling modulate triggered calcium, which could shorten APD (Shen and Zipes, 2014). At the tissue level, sympathetic drive reduces transmural dispersion of APs (Dukes and Vaughan Williams, 1984). If $I_{Ca,L}$ is selectively increased, all else remaining equal, the resulting ventricular APD would prolong, appearing on the ECG as a longer QT interval (Tranquillo and Sunkara, 2007). In cRadKO cardiomyocytes, increased LTCC peak current is offset by faster kinetics, thus raising the possibility that the net effect of Rad loss on cardiac electrophysiology for APD and QT prolongation is nullified (Manning et al., 2013; Figs. 7 and 11).

An alternative idea stems from Findlay, who proposed that modulation of LTCC from β-AR stimulation resulted in a switch from VDI to CDI. Under basal conditions, it was thought that CDI contributed to decay at more negative potentials, whereas VDI dominated as the membrane became more depolarized. Findlay and others showed that VDI has a biphasic decay and that rapid VDI contributes to the fast component of $I_{Ca,L}$, not just CDI (Findlay, 2002a; Findlay, 2004; Findlay, 2002c; Findlay, 2002b; Mitarai et al., 2000). However, in the presence of isoprenaline, CDI dominated at all voltages, and VDI was suppressed. Findlay's prediction was that CDI would then have little contribution to

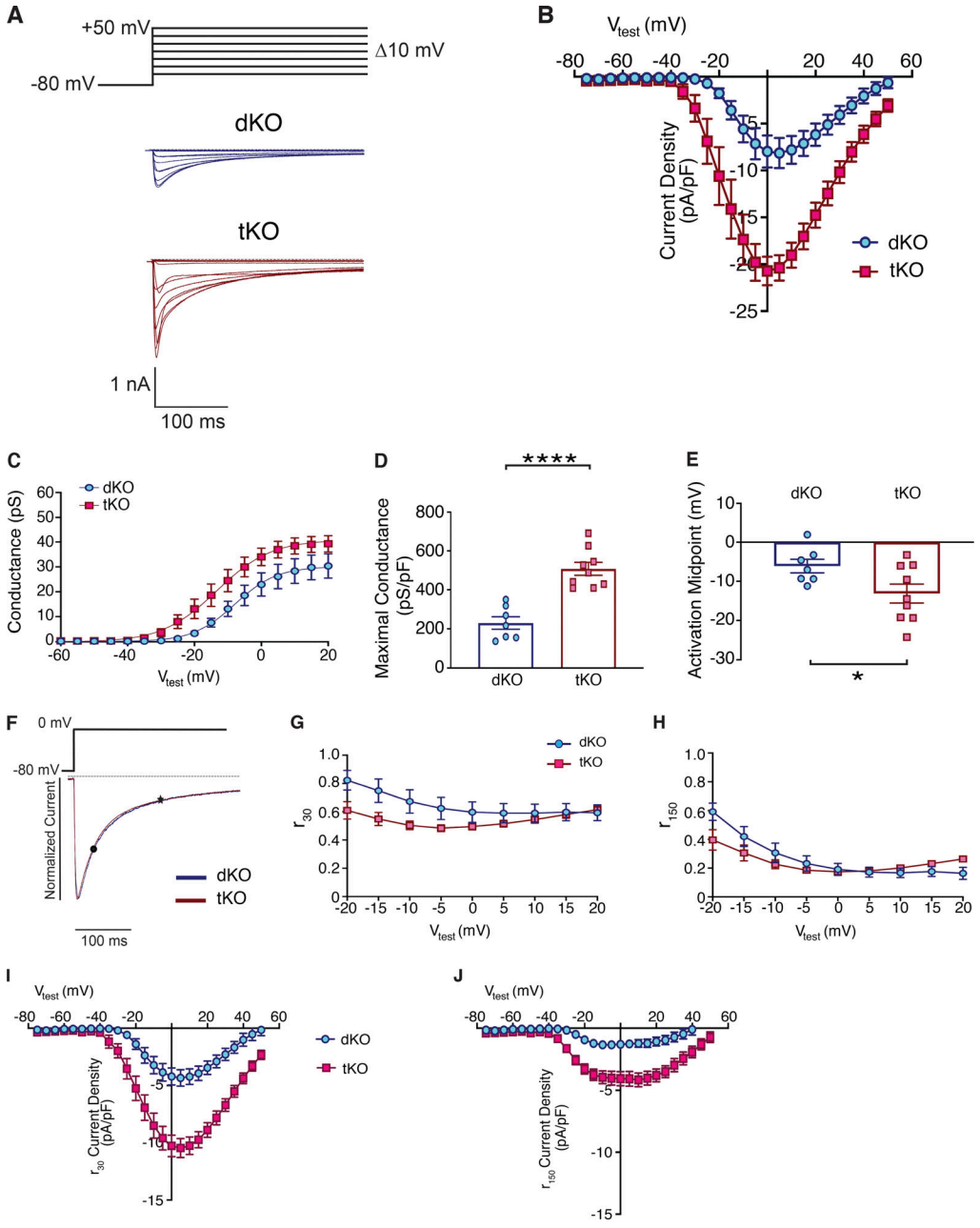

Figure 10. **Rad deletion yields modulated $I_{Ca,L}$ in the absence of $\beta_1\beta_2$-ARs. (A)** Exemplar family of Ca^{2+} currents of dKO (dark blue) and tKO (dark red). Scale bar, 1 nA, 100 ms. **(B)** Peak $I_{Ca,L}$ current density is larger in tKO than in dKO. **(C and D)** Conductance transform of I-V curve demonstrates higher maximal conductance in tKO than in dKO with quantification shown in D (****, P < 0.0001). **(E)** Activation midpoint is significantly negatively shifted in tKO (*, P = 0.04). **(F)** Exemplar Ca^{2+} currents with EGTA for dKO (dark blue) and tKO (dark red). Traces were normalized to peak current at 0 mV. Scale bar, 100 ms. Black dots indicate r_{30}. Black stars indicate r_{150}. **(G and H)** Remaining current across voltage steps 30 ms after peak (G) and 150 ms after peak (H). **(I and J)** $I_{Ca,L}$ current density 30 ms (I) and 150 ms (J) after peak. dKO: *n* = 3 mice, *n* = 7 cells; tKO: *n* = 3 mice, *n* = 9 cells. P values were calculated using Student's unpaired *t* test for D and E. Data in B–E and G–J are presented as mean ± SEM values. Data in G and H were analyzed by two-way ANOVA plus Šídák's multiple comparisons test.

the AP under basal conditions but could promote severe slowing of $I_{Ca,L}$ decay and therefore elongation of the AP after β-AR stimulation (Findlay, 2004). Our results demonstrate that the absence of Rad accelerates VDI in both the fast and slow components of $I_{Ca,L}$ decay (Fig. 6). This does not result in elongation of the AP, nor does it significantly prolong the QT interval (Fig. 7). It is therefore possible that Rad contributes to LTCC regulation by allowing this switch between VDI and CDI. Under basal conditions, the presence of Rad regulates VDI; when β-Ars are activated, Rad phosphorylation causes dissociation from the LTCC (Liu et al., 2020), and CDI then becomes the dominant inactivation mechanism as channels cluster together and elevate intracellular calcium. The synchronous activity of these clusters then promotes accelerated CDI so that the increase in $I_{Ca,L}$ is offset so as not to significantly alter APs. Further studies into how phosphorylation of Rad alters its location within the

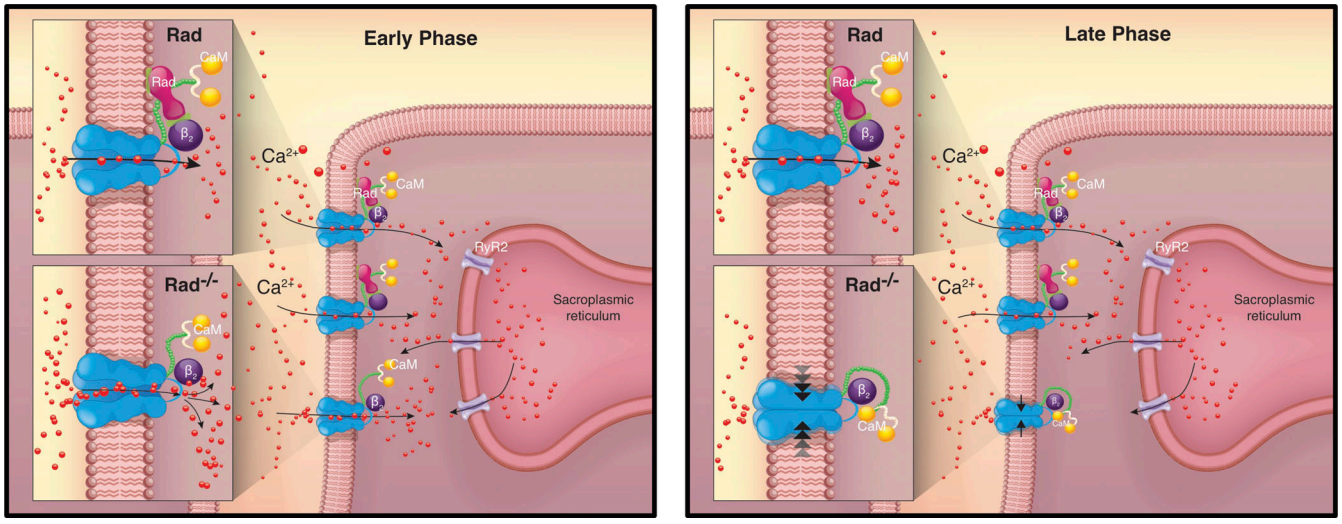

Figure 11. **Rad modulates $I_{Ca,L}$ independent of β-adrenergic signaling to confer systolic advantage.** The absence of Rad results in modulated $I_{Ca,L}$ that enhances cardiac contraction (early phase) without promoting electrical dysfunction because of accelerated decay kinetics (late phase).

complex or its interactions with other proteins could help elucidate how Rad contributes to LTCC inactivation, especially under conditions of β-AR stimulation.

Rad regulation of LTCC is independent of β-AR signaling

Our work has demonstrated that Rad is a critical component in LTCC modulation by β-AR stimulation (Ahern et al., 2019; Manning et al., 2013; Levitan et al., 2016). Indeed, cardiomyocyte-restricted Rad deletion demonstrates the extreme by which the loss of Rad yields maximally modulated $I_{Ca,L}$ that translates from channel function up to enhanced in vivo cardiac function. Data collected from the tKO demonstrated that the maximal modulation of $I_{Ca,L}$ is due to the absence of Rad from the LTCC, exclusive of activation of β-ARs (Figs. 9, 10, and 11). Others who have used β_1-AR knockout, β_2-AR knockout, or $\beta_1\beta_2$-AR dKO models have reported minimal impacts on basal cardiac function, suggesting that there are potentially other controls for critical physiological functions, such as cardiac rate and contractility, to compensate for the loss of these receptors (Xiang and Kobilka, 2003; Nikolaev et al., 2010; Myagmar et al., 2017; Rohrer et al., 1999; Jimenez et al., 2002; Devic et al., 2001). In $\beta_1\beta_2$-AR dKO neonatal myocytes, β_3-AR was shown to stimulate contraction after treatment with ISO, though desensitization occurred more rapidly than with β_1-AR or β_2-AR (Devic et al., 2001). It is therefore possible that there is a minor contribution from other sources to how the heart responds to increased sympathetic drive. However, our data clearly demonstrate a significant increase in function, both at the level of the whole heart and at the level of the channel, when Rad is deleted in the $\beta_1\beta_2$-AR dKO without significant prolongation of the QT interval. We have previously shown that Rad deletion allows a systolic advantage without promoting damaging effects that are normally associated with the chronic use of positive inotropes (Ahern et al., 2019; Manning et al., 2013). Therefore, we suggest that Rad reduction could serve as a treatment for heart failure that enhances systolic function while preserving β-AR signaling pathways and without increasing proarrhythmic late $I_{Ca,L}$ (Mahajan et al., 2008; Madhvani et al., 2011; Karagueuzian et al., 2017; Madhvani et al., 2015).

Limitations

It is possible that differential dispersed cell activity might arise from cellular damage artifact during enzymatic dispersal. However, our findings in this study are similar to those of other reports of Rad deletion on cardiac function (Finlin et al., 2003; Ahern et al., 2019; Manning et al., 2013; Liu et al., 2020). These studies are limited to the mouse. Mice have a larger SR calcium content and greater SERCA activity than those of larger species (Wang et al., 2019; Morotti et al., 2012). Repolarizing current is mostly carried by I_{to} and I_{Kur} in the mouse, whereas larger species express I_{Kr} and I_{Ks} (Wang et al., 2019). Despite these differences, the cardiac fight-or-flight response is conserved across multiple species, and this study gives further insight into how LTCC activity is modulated.

We have also not explored ion channel regulation in the absence of Rad other than that of LTCC regulation. Although there is no current evidence to suggest that Rad interacts with other channel complexes besides the LTCC, interactions may still exist. It is also possible that other ion channels that are affected by intracellular calcium could experience secondary effects due to Rad deletion. Indeed, it is possible, for example, that calcium-activated potassium channels could be activated in cRadKO so that balance is maintained in the plateau phase of the AP and the QT interval is not prolonged (Fig. 7). Further studies into the effect of Rad deletion on other ion channels may enhance understanding of the fight-or-flight response and how it is different or similar in other species.

Conclusions

In summary, we have demonstrated that modulation of the LTCC is governed by the presence of Rad in the $Ca_V1.2$ macromolecular complex. The absence of Rad yields an increase in peak $I_{Ca,L}$ that is offset by an increase in both VDI and CDI so that

AP and QT interval are not significantly prolonged. β-AR–mediated modulation of the LTCC is governed by Rad. Taken together, Rad reduction within cardiomyocytes is a compelling potential therapeutic approach for increasing cardiac function without the need for β-blockers, thereby improving quality and quantity of life for those with heart failure.

Acknowledgments

David A. Eisner served as editor.

The authors thank Dr. Brian Delisle for data analysis support and insightful discussion and Matthew Hazzard from the Medical Illustration Department of the University of Kentucky for creating the model illustration for this study (Fig. 11).

This research was funded by an American Heart Association predoctoral fellowship to B.M. Ahern (19PRE34380909), a National Institutes of Health/National Heart, Lung, and Blood Institute grant (HL131782), and a U.S. Department of Defense grant (W81WXH-20-1-0418).

The authors declare no competing financial interests.

Author contributions: B.M. Ahern, D.A. Andres, and J. Satin: conceptualization; B.M. Ahern, B.M. Levitan, and J. Goh: data curation; B.M. Ahern and J. Satin: formal analysis; B.M. Ahern, D.A. Andres, and J. Satin: supervision; B.M. Ahern, D.A. Andres, and J. Satin: funding acquisition; B.M. Ahern, A. Sebastian, and B.M. Levitan: investigation; B.M. Ahern and J. Satin: writing – original draft; B.M. Ahern, D.A. Andres, and J. Satin: project administration; D.A. Andres and J. Satin: resources.

Submitted: 16 December 2020
Accepted: 25 June 2021

References

Ahern, B.M., and J. Satin. 2019. The L-type calcium channel current modulation mechanism: the plot thickens and fogs. *J. Clin. Invest.* 129:496–498. https://doi.org/10.1172/JCI125958

Ahern, B.M., B.M. Levitan, S. Veeranki, M. Shah, N. Ali, A. Sebastian, W. Su, M.C. Gong, J. Li, J.E. Stelzer, et al. 2019. Myocardial-restricted ablation of the GTPase RAD results in a pro-adaptive heart response in mice. *J. Biol. Chem.* 294:10913–10927. https://doi.org/10.1074/jbc.RA119.008782

Alseikhan, B.A., C.D. DeMaria, H.M. Colecraft, and D.T. Yue. 2002. Engineered calmodulins reveal the unexpected eminence of Ca^{2+} channel inactivation in controlling heart excitation. *Proc. Natl. Acad. Sci. USA.* 99: 17185–17190. https://doi.org/10.1073/pnas.262372999

Bayer, K.U., P. De Koninck, A.S. Leonard, J.W. Hell, and H. Schulman. 2001. Interaction with the NMDA receptor locks CaMKII in an active conformation. *Nature.* 411:801–805. https://doi.org/10.1038/35081080

Bean, B.P., M.C. Nowycky, and R.W. Tsien. 1984. β-adrenergic modulation of calcium channels in frog ventricular heart cells. *Nature.* 307:371–375. https://doi.org/10.1038/307371a0

Béguin, P., K. Nagashima, T. Gonoi, T. Shibasaki, K. Takahashi, Y. Kashima, N. Ozaki, K. Geering, T. Iwanaga, and S. Seino. 2001. Regulation of Ca^{2+} channel expression at the cell surface by the small G-protein kir/Gem. *Nature.* 411:701–706. https://doi.org/10.1038/35079621

Benmocha Guggenheimer, A., L. Almagor, V. Tsemakhovich, D.R. Tripathy, J.A. Hirsch, and N. Dascal. 2016. Interactions between N and C termini of α1C subunit regulate inactivation of $Ca_V1.2$ L-type $Ca^{(2+)}$ channel. *Channels (Austin).* 10:55–68. https://doi.org/10.1080/19336950.2015.1108499

Bers, D.M. 2002. Cardiac excitation-contraction coupling. *Nature.* 415: 198–205. https://doi.org/10.1038/415198a

Breijo-Marquez, F.R., editor. 2012. Cardiac Arrhythmias: New Considerations. IntechOpen, Rijeka, Croatia. https://doi.org/10.5772/1454

Bryant, S., T.E. Kimura, C.H. Kong, J.J. Watson, A. Chase, M.S. Suleiman, A.F. James, and C.H. Orchard. 2014. Stimulation of ICa by basal PKA activity is facilitated by caveolin-3 in cardiac ventricular myocytes. *J. Mol. Cell. Cardiol.* 68:47–55. https://doi.org/10.1016/j.yjmcc.2013.12.026

Bryant, S.M., C.H.T. Kong, J.J. Watson, H.C. Gadeberg, D.M. Roth, H.H. Patel, M.B. Cannell, A.F. James, and C.H. Orchard. 2018. Caveolin-3 KO disrupts t-tubule structure and decreases t-tubular I_{Ca} density in mouse ventricular myocytes. *Am. J. Physiol. Heart Circ. Physiol.* 315:H1101–H1111. https://doi.org/10.1152/ajpheart.00209.2018

Chen, X., H. Nakayama, X. Zhang, X. Ai, D.M. Harris, M. Tang, H. Zhang, C. Szeto, K. Stockbower, R.M. Berretta, et al. 2011. Calcium influx through Cav1.2 is a proximal signal for pathological cardiomyocyte hypertrophy. *J. Mol. Cell. Cardiol.* 50:460–470. https://doi.org/10.1016/j.yjmcc.2010.11.012

Chruscinski, A.J., D.K. Rohrer, E. Schauble, K.H. Desai, D. Bernstein, and B.K. Kobilka. 1999. Targeted disruption of the β2 adrenergic receptor gene. *J. Biol. Chem.* 274:16694–16700. https://doi.org/10.1074/jbc.274.24.16694

Correll, R.N., C. Pang, D.M. Niedowicz, B.S. Finlin, and D.A. Andres. 2008. The RGK family of GTP-binding proteins: regulators of voltage-dependent calcium channels and cytoskeleton remodeling. *Cell. Signal.* 20:292–300. https://doi.org/10.1016/j.cellsig.2007.10.028

Devic, E., Y. Xiang, D. Gould, and B. Kobilka. 2001. β-adrenergic receptor subtype-specific signaling in cardiac myocytes from $\beta(_1)$ and $\beta(_2)$ adrenoceptor knockout mice. *Mol. Pharmacol.* 60:577–583.

Dixon, R.E., C. Yuan, E.P. Cheng, M.F. Navedo, and L.F. Santana. 2012. Ca^{2+} signaling amplification by oligomerization of L-type Cav1.2 channels. *Proc. Natl. Acad. Sci. USA.* 109:1749–1754. https://doi.org/10.1073/pnas.1116731109

Dixon, R.E., C.M. Moreno, C. Yuan, X. Opitz-Araya, M.D. Binder, M.F. Navedo, and L.F. Santana. 2015. Graded Ca^{2+}/calmodulin-dependent coupling of voltage-gated CaV1.2 channels. *eLife.* 4:e05608. https://doi.org/10.7554/eLife.05608

Dukes, I.D., and E.M. Vaughan Williams. 1984. Effects of selective α_1-, α_2-, β_1- and β_2-adrenoceptor stimulation on potentials and contractions in the rabbit heart. *J. Physiol.* 355:523–546. https://doi.org/10.1113/jphysiol.1984.sp015436

Fakler, B., and J.P. Adelman. 2008. Control of $K(_{Ca})$ channels by calcium nano/microdomains. *Neuron.* 59:873–881. https://doi.org/10.1016/j.neuron.2008.09.001

Findlay, I. 2002a. Voltage-dependent inactivation of L-type Ca^{2+} currents in guinea-pig ventricular myocytes. *J. Physiol.* 545:389–397. https://doi.org/10.1113/jphysiol.2002.029637

Findlay, I. 2002b. β-adrenergic and muscarinic agonists modulate inactivation of L-type Ca^{2+} channel currents in guinea-pig ventricular myocytes. *J. Physiol.* 545:375–388. https://doi.org/10.1113/jphysiol.2002.028605

Findlay, I. 2002c. β-Adrenergic stimulation modulates Ca^{2+}- and voltage-dependent inactivation of L-type Ca^{2+} channel currents in guinea-pig ventricular myocytes. *J. Physiol.* 541:741–751. https://doi.org/10.1113/jphysiol.2002.019737

Findlay, I. 2004. Physiological modulation of inactivation in L-type Ca^{2+} channels: one switch. *J. Physiol.* 554:275–283. https://doi.org/10.1113/jphysiol.2003.047902

Finlin, B.S., S.M. Crump, J. Satin, and D.A. Andres. 2003. Regulation of voltage-gated calcium channel activity by the Rem and Rad GTPases. *Proc. Natl. Acad. Sci. USA.* 100:14469–14474. https://doi.org/10.1073/pnas.2437756100

Grandi, E., S. Morotti, K.S. Ginsburg, S. Severi, and D.M. Bers. 2010. Interplay of voltage and Ca-dependent inactivation of L-type Ca current. *Prog. Biophys. Mol. Biol.* 103:44–50. https://doi.org/10.1016/j.pbiomolbio.2010.02.001

Gunton, J.E., M. Sisavanh, R.A. Stokes, J. Satin, L.S. Satin, M. Zhang, S.M. Liu, W. Cai, K. Cheng, G.J. Cooney, et al. 2012. Mice deficient in GEM GTPase show abnormal glucose homeostasis due to defects in beta-cell calcium handling. *PLoS One.* 7:e39462. https://doi.org/10.1371/journal.pone.0039462

Han, D., X. Xue, Y. Yan, and G. Li. 2019. Dysfunctional Cav1.2 channel in Timothy syndrome, from cell to bedside. *Exp. Biol. Med. (Maywood).* 244: 960–971. https://doi.org/10.1177/1535370219863149

Ito, D.W., K.I. Hannigan, D. Ghosh, B. Xu, S.G. Del Villar, Y.K. Xiang, E.J. Dickson, M.F. Navedo, and R.E. Dixon. 2019. β-adrenergic-mediated dynamic augmentation of sarcolemmal Ca_V 1.2 clustering and cooperativity in ventricular myocytes. *J. Physiol.* 597:2139–2162. https://doi.org/10.1113/JP277283

Ivanina, T., Y. Blumenstein, E. Shistik, R. Barzilai, and N. Dascal. 2000. Modulation of L-type Ca2+ channels by gbeta γ and calmodulin via

interactions with N and C termini of α 1C. *J. Biol. Chem.* 275: 39846–39854. https://doi.org/10.1074/jbc.M005881200

January, C.T., and J.M. Riddle. 1989. Early afterdepolarizations: mechanism of induction and block. A role for L-type Ca^{2+} current. *Circ. Res.* 64: 977–990. https://doi.org/10.1161/01.RES.64.5.977

January, C.T., J.M. Riddle, and J.J. Salata. 1988. A model for early afterdepolarizations: induction with the Ca^{2+} channel agonist Bay K 8644. *Circ. Res.* 62:563–571. https://doi.org/10.1161/01.RES.62.3.563

Jimenez, M., B. Léger, K. Canola, L. Lehr, P. Arboit, J. Seydoux, A.P. Russell, J.-P. Giacobino, P. Muzzin, and F. Preitner. 2002. $\beta_{(1)}/\beta_{(2)}/\beta_{(3)}$-adrenoceptor knockout mice are obese and cold-sensitive but have normal lipolytic responses to fasting. *FEBS Lett.* 530:37–40. https://doi.org/10.1016/S0014-5793(02)03387-2

Karagueuzian, H.S., A. Pezhouman, M. Angelini, and R. Olcese. 2017. Enhanced late Na and Ca currents as effective antiarrhythmic drug targets. *Front. Pharmacol.* 8:36. https://doi.org/10.3389/fphar.2017.00036

Lacinová, L., and F. Hofmann. 2005. Ca^{2+}- and voltage-dependent inactivation of the expressed L-type $Ca_{(v)}1.2$ calcium channel. *Arch. Biochem. Biophys.* 437:42–50. https://doi.org/10.1016/j.abb.2005.02.025

Lei, M., J. Xu, Q. Gao, E. Minobe, M. Kameyama, and L. Hao. 2018. PKA phosphorylation of Cav1.2 channel modulates the interaction of calmodulin with the C terminal tail of the channel. *J. Pharmacol. Sci.* 137: 187–194. https://doi.org/10.1016/j.jphs.2018.05.010

Levitan, B.M., J.R. Manning, C.N. Withers, J.D. Smith, R.M. Shaw, D.A. Andres, V.L. Sorrell, and J. Satin. 2016. Rad-deletion phenocopies tonic sympathetic stimulation of the heart. *J. Cardiovasc. Transl. Res.* 9: 432–444. https://doi.org/10.1007/s12265-016-9716-y

Liu, G., A. Papa, A.N. Katchman, S.I. Zakharov, D. Roybal, J.A. Hennessey, J. Kushner, L. Yang, B.-X. Chen, A. Kushnir, et al. 2020. Mechanism of adrenergic $Ca_V1.2$ stimulation revealed by proximity proteomics. *Nature.* 577:695–700. https://doi.org/10.1038/s41586-020-1947-z

Madhvani, R.V., Y. Xie, A. Pantazis, A. Garfinkel, Z. Qu, J.N. Weiss, and R. Olcese. 2011. Shaping a new Ca^{2+} conductance to suppress early afterdepolarizations in cardiac myocytes. *J. Physiol.* 589:6081–6092. https://doi.org/10.1113/jphysiol.2011.219600

Madhvani, R.V., M. Angelini, Y. Xie, A. Pantazis, S. Suriany, N.P. Borgstrom, A. Garfinkel, Z. Qu, J.N. Weiss, and R. Olcese. 2015. Targeting the late component of the cardiac L-type Ca^{2+} current to suppress early afterdepolarizations. *J. Gen. Physiol.* 145:395–404. https://doi.org/10.1085/jgp.201411288

Magyar, J., C.E. Kiper, G. Sievert, W. Cai, G.-X. Shi, S.M. Crump, L. Li, S. Niederer, N. Smith, D.A. Andres, and J. Satin. 2012. Rem-GTPase regulates cardiac myocyte L-type calcium current. *Channels (Austin).* 6: 166–173. https://doi.org/10.4161/chan.20192

Mahajan, A., D. Sato, Y. Shiferaw, A. Baher, L.-H. Xie, R. Peralta, R. Olcese, A. Garfinkel, Z. Qu, and J.N. Weiss. 2008. Modifying L-type calcium current kinetics: consequences for cardiac excitation and arrhythmia dynamics. *Biophys. J.* 94:411–423. https://doi.org/10.1529/biophysj.106.98590

Manning, J.R., G. Yin, C.N. Kaminski, J. Magyar, H.-Z. Feng, J. Penn, G. Sievert, K. Thompson, J.-P. Jin, D.A. Andres, and J. Satin. 2013. Rad GTPase deletion increases L-type calcium channel current leading to increased cardiac contraction. *J. Am. Heart Assoc.* 2:e000459. https://doi.org/10.1161/JAHA.113.000459

Manning, J.R., C.N. Withers, B. Levitan, J.D. Smith, D.A. Andres, and J. Satin. 2015. Loss of Rad-GTPase produces a novel adaptive cardiac phenotype resistant to systolic decline with aging. *Am. J. Physiol. Heart Circ. Physiol.* 309:H1336–H1345. https://doi.org/10.1152/ajpheart.00389.2015

Markandeya, Y.S., and T.J. Kamp. 2015. Rational strategy to stop arrhythmias: Early afterdepolarizations and L-type Ca^{2+} current. *J. Gen. Physiol.* 145: 475–479. https://doi.org/10.1085/jgp.201511429

Mitarai, S., M. Kaibara, K. Yano, and K. Taniyama. 2000. Two distinct inactivation processes related to phosphorylation in cardiac L-type $Ca^{(2+)}$ channel currents. *Am. J. Physiol. Cell Physiol.* 279:C603–C610. https://doi.org/10.1152/ajpcell.2000.279.3.C603

Morales, D., T. Hermosilla, and D. Varela. 2019. Calcium-dependent inactivation controls cardiac L-type Ca^{2+} currents under β-adrenergic stimulation. *J. Gen. Physiol.* 151:786–797. https://doi.org/10.1085/jgp.201812236

Morotti, S., E. Grandi, A. Summa, K.S. Ginsburg, and D.M. Bers. 2012. Theoretical study of L-type $Ca^{(2+)}$ current inactivation kinetics during action potential repolarization and early afterdepolarizations. *J. Physiol.* 590:4465–4481. https://doi.org/10.1113/jphysiol.2012.231886

Muth, J.N., H. Yamaguchi, G. Mikala, I.L. Grupp, W. Lewis, H. Cheng, L.-S. Song, E.G. Lakatta, G. Varadi, and A. Schwartz. 1999. Cardiac-specific overexpression of the $\alpha_{(1)}$ subunit of the L-type voltage-dependent $Ca^{(2+)}$ channel in transgenic mice. Loss of isoproterenol-induced contraction. *J. Biol. Chem.* 274:21503–21506. https://doi.org/10.1074/jbc.274.31.21503

Myagmar, B.-E., J.M. Flynn, P.M. Cowley, P.M. Swigart, M.D. Montgomery, K. Thai, D. Nair, R. Gupta, D.X. Deng, C. Hosoda, et al. 2017. Adrenergic receptors in individual ventricular myocytes: the beta-1 and alpha-1B are in all cells, the alpha-1A is in a subpopulation, and the beta-2 and beta-3 are mostly absent. *Circ. Res.* 120:1103–1115. https://doi.org/10.1161/CIRCRESAHA.117.310520

Naraghi, M., and E. Neher. 1997. Linearized buffered Ca^{2+} diffusion in microdomains and its implications for calculation of $[Ca^{2+}]$ at the mouth of a calcium channel. *J. Neurosci.* 17:6961–6973. https://doi.org/10.1523/JNEUROSCI.17-18-06961.1997

Navedo, M.F., E.P. Cheng, C. Yuan, S. Votaw, J.D. Molkentin, J.D. Scott, and L.F. Santana. 2010. Increased coupled gating of L-type Ca^{2+} channels during hypertension and Timothy syndrome. *Circ. Res.* 106:748–756. https://doi.org/10.1161/CIRCRESAHA.109.213363

Nikolaev, V.O., A. Moshkov, A.R. Lyon, M. Miragoli, P. Novak, H. Paur, M.J. Lohse, Y.E. Korchev, S.E. Harding, and J. Gorelik. 2010. β_2-adrenergic receptor redistribution in heart failure changes cAMP compartmentation. *Science.* 327:1653–1657. https://doi.org/10.1126/science.1185988

Pallien, T., and E. Klussmann. 2020. New aspects in cardiac L-type Ca^{2+} channel regulation. *Biochem. Soc. Trans.* 48:39–49. https://doi.org/10.1042/BST20190229

Pelzer, D., S. Pelzer, and T.F. McDonald. 1990. Properties and regulation of calcium channels in muscle cells. *Rev. Physiol. Biochem. Pharmacol.* 114: 107–207. https://doi.org/10.1007/BFb0031019

Peterson, B.Z., C.D. DeMaria, J.P. Adelman, and D.T. Yue. 1999. Calmodulin is the Ca^{2+} sensor for Ca^{2+} -dependent inactivation of L-type calcium channels. *Neuron.* 22:549–558. https://doi.org/10.1016/S0896-6273(00)80709-6

Rohrer, D.K., A. Chruscinski, E.H. Schauble, D. Bernstein, and B.K. Kobilka. 1999. Cardiovascular and metabolic alterations in mice lacking both β_1- and β_2-adrenergic receptors. *J. Biol. Chem.* 274:16701–16708. https://doi.org/10.1074/jbc.274.24.16701

Shen, M.J., and D.P. Zipes. 2014. Role of the autonomic nervous system in modulating cardiac arrhythmias. *Circ. Res.* 114:1004–1021. https://doi.org/10.1161/CIRCRESAHA.113.302549

Sheng, X., T. Nakada, M. Kobayashi, T. Kashihara, T. Shibazaki, M. Horiuchi-Hirose, S. Gomi, M. Hirose, T. Aoyama, and M. Yamada. 2012. Two mechanistically distinct effects of dihydropyridine nifedipine on CaV1.2 L-type Ca^{2+} channels revealed by Timothy syndrome mutation. *Eur. J. Pharmacol.* 685:15–23. https://doi.org/10.1016/j.ejphar.2012.04.029

Splawski, I., K.W. Timothy, L.M. Sharpe, N. Decher, P. Kumar, R. Bloise, C. Napolitano, P.J. Schwartz, R.M. Joseph, K. Condouris, et al. 2004. $Ca_{(V)}$ 1.2 calcium channel dysfunction causes a multisystem disorder including arrhythmia and autism. *Cell.* 119:19–31. https://doi.org/10.1016/j.cell.2004.09.011

Splawski, I., K.W. Timothy, N. Decher, P. Kumar, F.B. Sachse, A.H. Beggs, M.C. Sanguinetti, and M.T. Keating. 2005. Severe arrhythmia disorder caused by cardiac L-type calcium channel mutations. *Proc. Natl. Acad. Sci. USA.* 102:8089–8096. https://doi.org/10.1073/pnas.0502506102

Tadross, M.R., I.E. Dick, and D.T. Yue. 2008. Mechanism of local and global Ca^{2+} sensing by calmodulin in complex with a Ca^{2+} channel. *Cell.* 133: 1228–1240. https://doi.org/10.1016/j.cell.2008.05.025

Tranquillo, J., and A. Sunkara. 2007. Can we trust the transgenic mouse? Insights from computer simulations. *In* Functional Imaging and Modeling of the Heart. FIMH 2007. Vol. 4466. F.B. Sachse, and G. Seemann, editors. Springer, Berlin, Heidelberg. 210–219. https://doi.org/10.1007/978-3-540-72907-5_22

Wang, L., S. Morotti, S. Tapa, S.D. Francis Stuart, Y. Jiang, Z. Wang, R.C. Myles, K.E. Brack, G.A. Ng, D.M. Bers, et al. 2019. Different paths, same destination: divergent action potential responses produce conserved cardiac fight-or-flight response in mouse and rabbit hearts. *J. Physiol.* 597:3867–3883. https://doi.org/10.1113/JP278016

Wickman, K., J. Nemec, S.J. Gendler, and D.E. Clapham. 1998. Abnormal heart rate regulation in GIRK4 knockout mice. *Neuron.* 20:103–114. https://doi.org/10.1016/S0896-6273(00)80438-9

Xiang, Y., and B.K. Kobilka. 2003. Myocyte adrenoceptor signaling pathways. *Science.* 300:1530–1532. https://doi.org/10.1126/science.1079206

Yang, T., and H.M. Colecraft. 2013. Regulation of voltage-dependent calcium channels by RGK proteins. *Biochim. Biophys. Acta.* 1828:1644–1654. https://doi.org/10.1016/j.bbamem.2012.10.005

Yarotskyy, V., and K.S. Elmslie. 2007. Roscovitine, a cyclin-dependent kinase inhibitor, affects several gating mechanisms to inhibit cardiac L-type

($Ca_{(V)}1.2$) calcium channels. *Br. J. Pharmacol.* 152:386–395. https://doi.org/10.1038/sj.bjp.0707414

Yarotskyy, V., G. Gao, B.Z. Peterson, and K.S. Elmslie. 2009. The Timothy syndrome mutation of cardiac $Ca_V1.2$ (L-type) channels: multiple altered gating mechanisms and pharmacological restoration of inactivation. *J. Physiol.* 587:551–565. https://doi.org/10.1113/jphysiol.2008.161737

Yazawa, M., B. Hsueh, X. Jia, A.M. Pasca, J.A. Bernstein, J. Hallmayer, and R.E. Dolmetsch. 2011. Using induced pluripotent stem cells to investigate cardiac phenotypes in Timothy syndrome. *Nature.* 471:230–234. https://doi.org/10.1038/nature09855

Zamponi, G.W. 2003. Calmodulin lobotomized: novel insights into calcium regulation of voltage-gated calcium channels. *Neuron.* 39:879–881. https://doi.org/10.1016/S0896-6273(03)00564-6

Zühlke, R.D., G.S. Pitt, K. Deisseroth, R.W. Tsien, and H. Reuter. 1999. Calmodulin supports both inactivation and facilitation of L-type calcium channels. *Nature.* 399:159–162. https://doi.org/10.1038/20200

Supplemental material

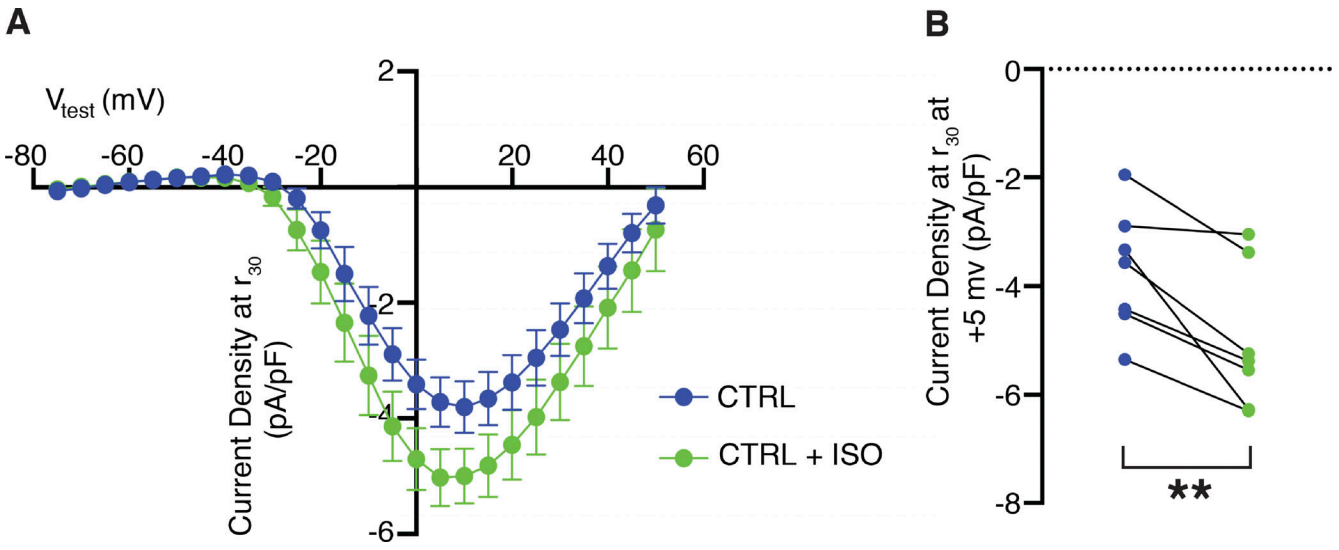

Figure S1. **ISO effect on CTRL $I_{Ca,L}$. (A)** CTRL $I_{Ca,L}$ current density 30 ms after peak before and after treatment with ISO. **(B)** ISO significantly increased current density at r_{30} in CTRL (at +5 mV; **, P = 0.007). CTRL: *n* = 4 mice, *n* = 7 cells. Data in A are presented as mean ± SEM values.

A

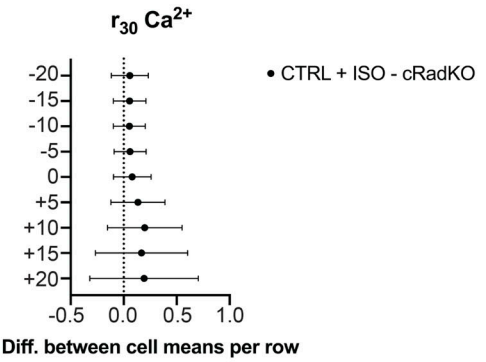

Source of Variation	P value	P value Summary	F (DFn, DFd)
Voltage	0.0027	**	F(1.558,43.43) = 7.786
CTRL + ISO v cRadKO	0.1032	ns	F(1,28) = 2.838
Voltage x CTRL + ISO v cRadKO	0.0009	***	F(8,223) = 3.436

B

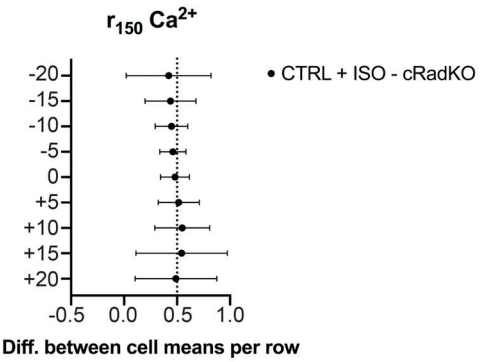

Source of Variation	P value	P value Summary	F (DFn, DFd)
Voltage	<0.0001	****	F(2.062,57.21) = 14.71
CTRL + ISO v cRadKO	0.7312	ns	F(1,28) = .1204
Voltage x CTRL + ISO v cRadKO	0.0071	**	F(8,222) = 2.717

C

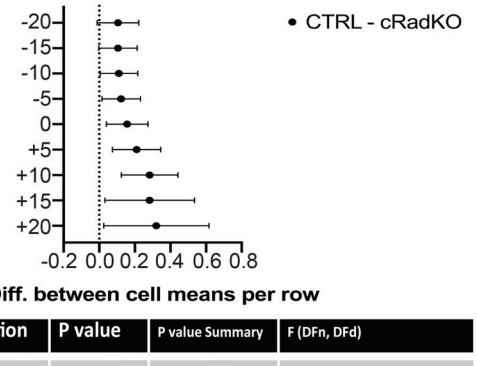

Source of Variation	P value	P value Summary	F (DFn, DFd)
Voltage	0.0344	*	F(1.402,58.52) = 4.101
CTRL v cRadKO	0.0002	***	F(1,42) = 17.35
Voltage x CTRL v cRadKO	<0.0001	****	F(8,334) = 6.576

D

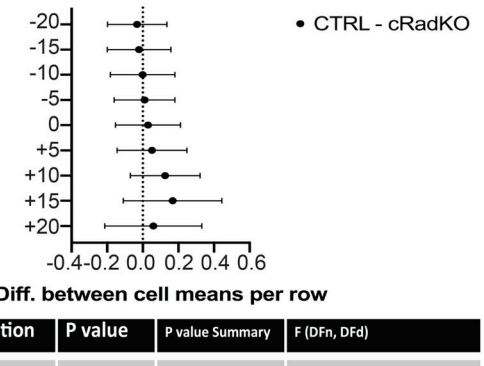

Source of Variation	P value	P value Summary	F (DFn, DFd)
Voltage	<0.0001	****	F(1.896,24.64) = 17.60
CTRL v cRadKO	0.3307	ns	F(1,13) = 1.021
Voltage x CTRL v cRadKO	0.0252	*	F(8,104) = 2.314

E

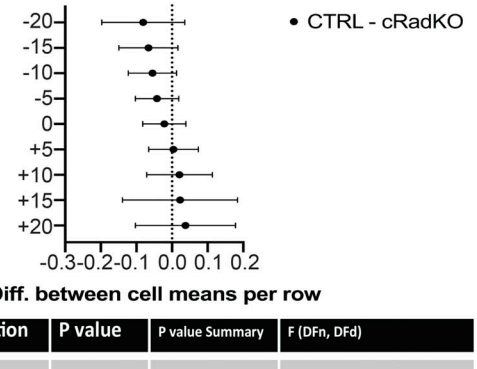

Source of Variation	P value	P value Summary	F (DFn, DFd)
Voltage	<0.0001	****	F(2.892,131.6) = 26.93
CTRL v cRadKO	0.4449	ns	F(1,46) = .5937
Voltage x CTRL v cRadKO	0.0009	***	F(8,364) = 3.406

F

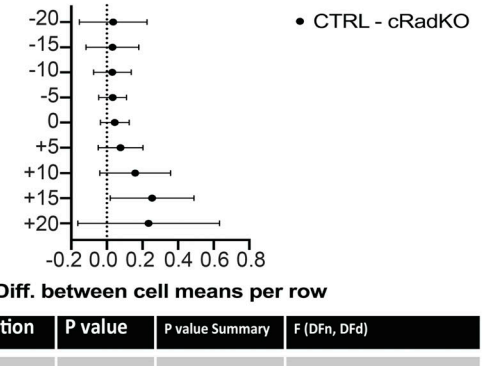

Source of Variation	P value	P value Summary	F (DFn, DFd)
Voltage	<0.0001	****	F(1.851,24.07) = 21.07
CTRL v cRadKO	0.0052	**	F(1,13) = 11.23
Voltage x CTRL v cRadKO	0.0027	**	F(8,104) = 3.204

Figure S2. **Two-way ANOVA 95% confidence intervals and tabular results. (A)** 95% confidence intervals and tabular results for Fig. 1 B. **(B)** 95% confidence intervals and tabular results for Fig. 1 C. **(C)** 95% confidence intervals and tabular results for Fig. 2 B. **(D)** 95% confidence intervals and tabular results for Fig. 3 B. **(E)** 95% confidence intervals and tabular results for Fig. 5 A. **(F)** 95% confidence intervals and tabular results for Fig. 5 D. Data are presented as mean ± 95% confidence intervals.*, P < 0.05; **, P < 0.01; ***, P < 0.001; ****, P < 0.0001. DFn and DFd are degrees of freedom in the numberator and demoninator, respectively.

A

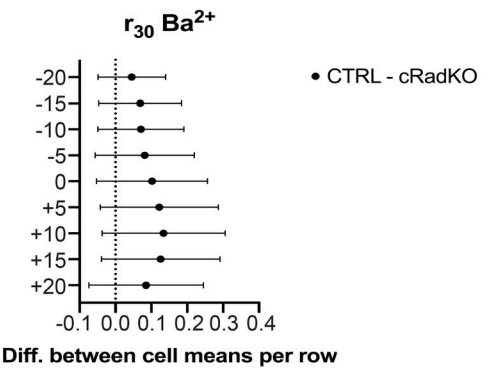

Source of Variation	P value	P value Summary	F (DFn, DFd)
Voltage	0.0011	**	F(2.352,30.58) = 7.807
CTRL v cRadKO	0.0388	*	F(1,13) = 5.279
Voltage x CTRL v cRadKO	0.0002	***	F(8,104) = 4.156

B

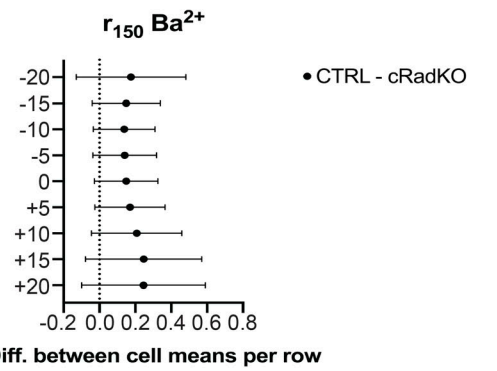

Source of Variation	P value	P value Summary	F (DFn, DFd)
Voltage	0.0055	**	F(2.266,29.46) = 5.880
CTRL v cRadKO	0.0081	**	F(1,13) = 9.756
Voltage x CTRL v cRadKO	0.4161	ns	F(8,104) = 1.033

C

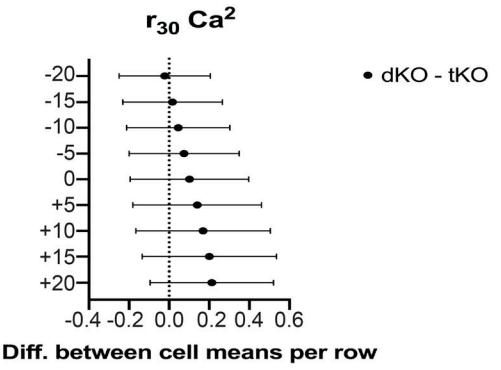

Source of Variation	P value	P value Summary	F (DFn, DFd)
Voltage	0.0047	**	F(1.256,17.58) =9.313
CTRL v cRadKO	0.1299	ns	F(1,14) = 2.589
Voltage x CTRL v cRadKO	<0.0001	****	F(8,112) = 5.205

D

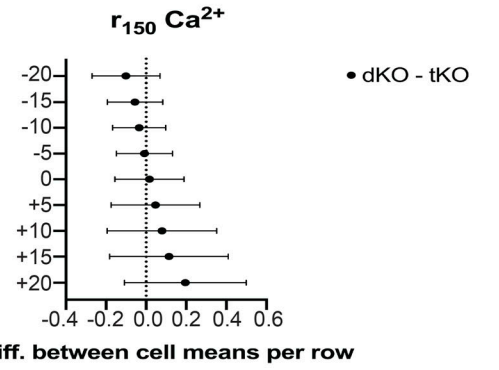

Source of Variation	P value	P value Summary	F (DFn, DFd)
Voltage	<0.0001	****	F(1.274,17.84) = 25.54
CTRL v cRadKO	0.5203	ns	F(1,14) = .4350
Voltage x CTRL v cRadKO	<0.0001	****	F(8,112) = 4.678

Figure S3. **Two-way ANOVA 95% confidence intervals and tabular results. (A)** 95% confidence intervals and tabular results for Fig. 6 B. **(B)** 95% confidence intervals and tabular results for Fig. 6 C. **(C)** 95% confidence intervals and tabular results for Fig. 10 G. **(D)** 95% confidence intervals and tabular results for Fig. 10 H. Data are presented as mean ± 95% confidence intervals.

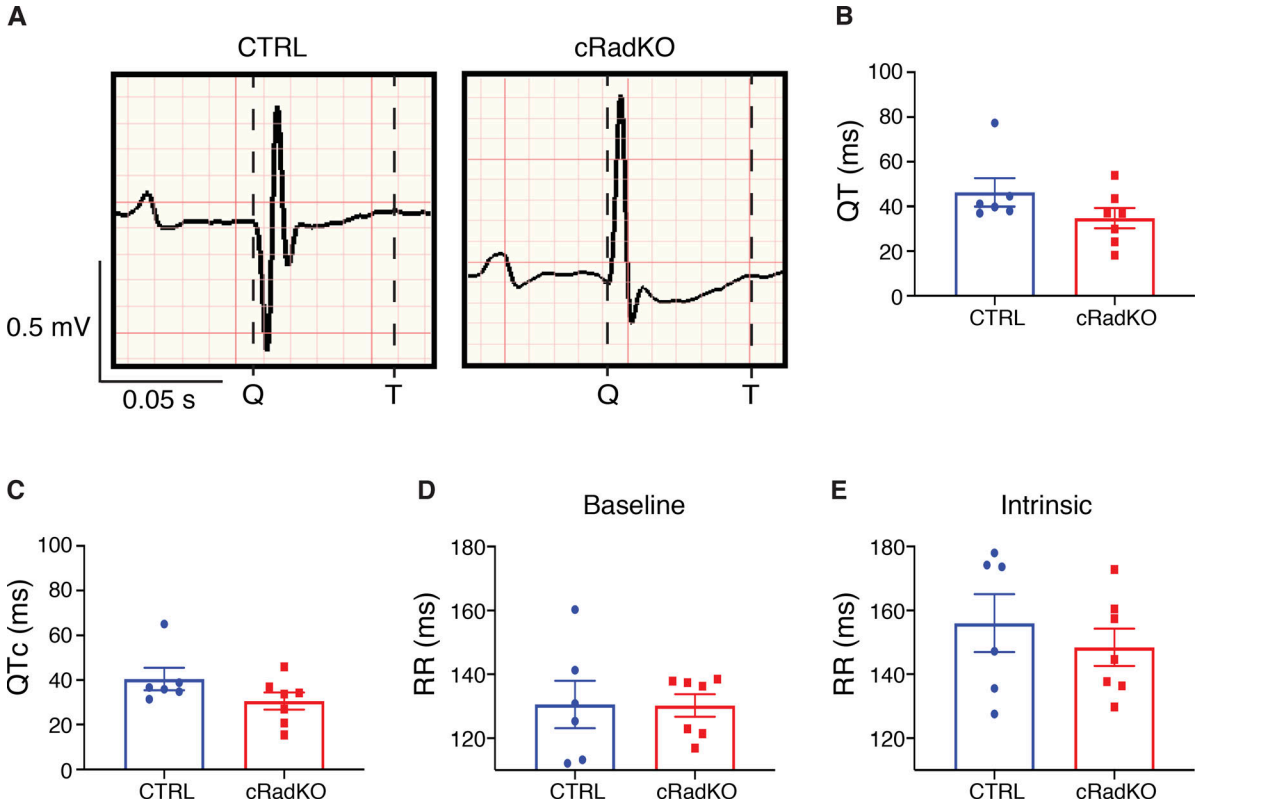

Figure S4. **Surface ECG measurements. (A)** Representative raw QT interval of baseline heart rate from surface ECG of CTRL and cRadKO. Scale bar, 0.5 mV, 50 ms. **(B)** Raw QT interval (ms) is not significantly different (P = 0.16). **(C)** QTc (ms) is not significantly different (P = 0.14). **(D)** Baseline R-R interval (ms) is not significantly different (P = 0.97). **(E)** Intrinsic R-R interval (ms) is not significantly different (P = 0.48) CTRL: *n* = 6 mice; cRadKO: *n* = 7 mice. P values calculated using Student's unpaired *t* test for B–E. Data in B–E are presented as mean ± SEM values.

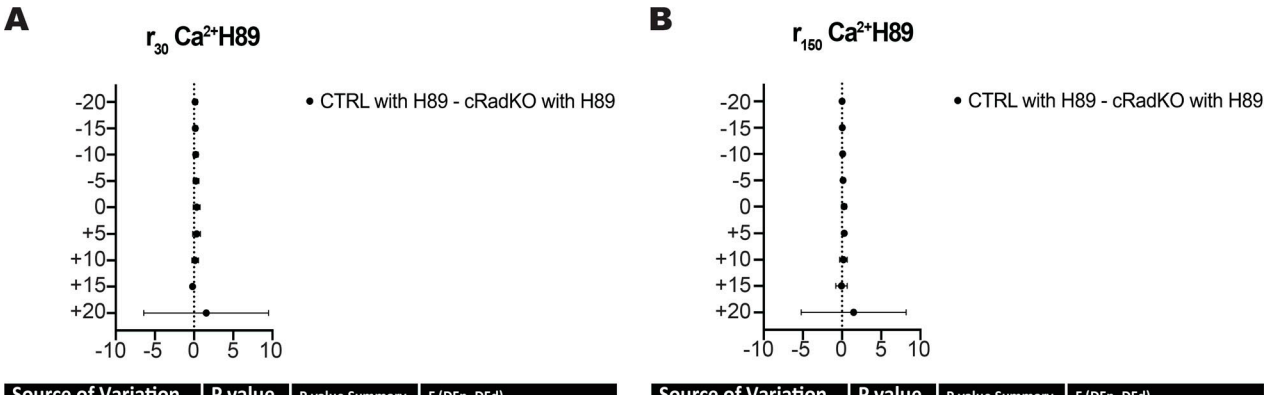

Source of Variation	P value	P value Summary	F (DFn, DFd)
Voltage	0.1411	ns	F(1.022,13.28) = 2.445
CTRL v cRadKO	0.0932	ns	F(1,13) = 3.281
Voltage x CTRL v cRadKO	0.3491	ns	F(8,104) = 1.131

Source of Variation	P value	P value Summary	F (DFn, DFd)
Voltage	0.0748	ns	F(1.026,13.59) = 3.702
CTRL v cRadKO	0.0632	ns	F(1,106) = .3.526
Voltage x CTRL v cRadKO	0.2670	ns	F(8,106) = 1.270

Figure S5. **Two-way ANOVA 95% confidence intervals and tabular results. (A)** 95% confidence intervals and tabular results for Fig. 8 E. **(B)** 95% confidence intervals and tabular results for Fig. 8 F.

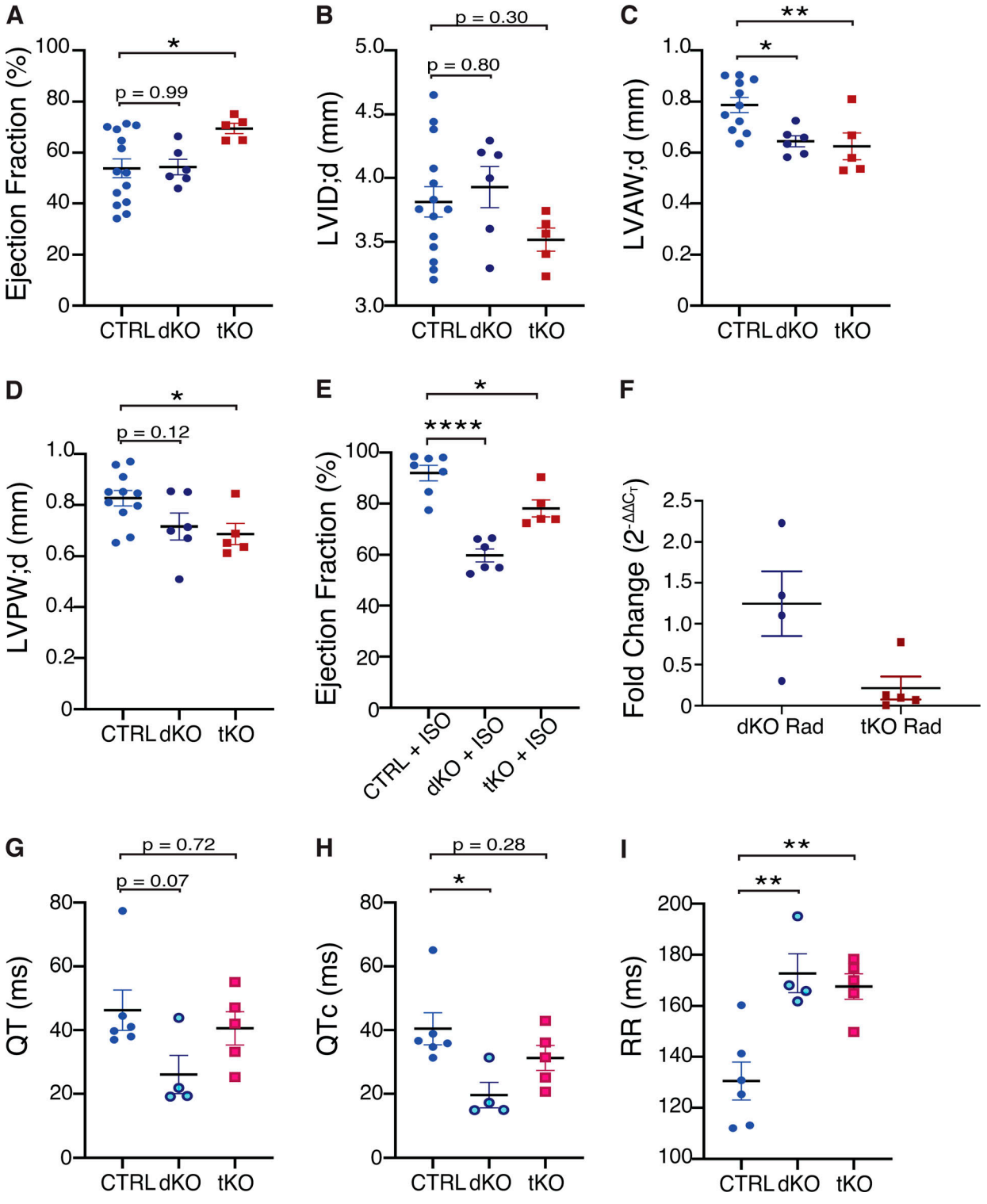

Figure S6. **Whole-heart measurements of dKO and tKO. (A)** Ejection fraction (*, P = 0.03). **(B)** Left ventricular inner dimensions in diastole (LVID;d). **(C)** Left ventricular anterior wall thickness; diastole (LVAW;d; *, P = 0.01; **, P = 0.009). **(D)** Left ventricular posterior wall thickness; diastole (LVPW;d; *, P = 0.05). **(E)** Ejection fraction after acute ISO (30 mg/kg) administration. Data for CTRL + ISO taken from published dataset in Ahern et al. (2019). *, P = 0.01; ****, P < 0.0001. **(F)** qRT-PCR analysis of samples from dKO and tKO hearts. **(G)** Raw QT interval. **(H)** QTc qRT-PCR analysis of samples from dKO and tKO hearts. G shows raw QT interval, and H shows QTc.